Downhill from Austin and Ely to Las Vegas: U-Pb detrital zircon suites from the Eocene–Oligocene Titus Canyon Formation and associated strata, Death Valley, California

Elizabeth L. Miller
Mark E. Raftrey*
Department of Geological Sciences, Stanford University, Stanford, California 94305, USA

Jens-Erik Lund Snee[†]
Department of Geophysics, Stanford University, Stanford, California 94305, USA

ABSTRACT

In a reconnaissance investigation aimed at interrogating the changing topography and paleogeography of the western United States prior to Basin and Range faulting, a preliminary study made use of U-Pb ages of detrital zircon suites from 16 samples from the Eocene–Oligocene Titus Canyon Formation, its overlying units, and correlatives near Death Valley. The Titus Canyon Formation unconformably overlies Neoproterozoic to Devonian strata in the Funeral and Grapevine Mountains of California and Nevada. Samples were collected from (1) the type area in Titus Canyon, (2) the headwaters of Monarch Canyon, and (3) unnamed Cenozoic strata exposed in a klippe of the Boundary Canyon fault in the central Funeral Mountains. Red beds and conglomerates at the base of the Titus Canyon Formation at locations 1 and 2, which contain previously reported 38–37 Ma fossils, yielded mostly Sierran batholith–age detrital zircons (defined by Triassic, Jurassic, and Cretaceous peaks). Overlying channelized fluvial sandstones, conglomerates, and minor lacustrine shale, marl, and limestone record an abrupt change in source region around 38–36 Ma or slightly later, from more local, Sierran arc–derived sediment to extraregional sources to the north. Clasts of red radiolarian-bearing chert, dark radiolarian chert, and quartzite indicate sources in the region of the Golconda and Roberts Mountains allochthons of northern Nevada. Sandstones intercalated with conglomerate contain increasing proportions of Cenozoic zircon sourced from south-migrating, caldera-forming eruptions at the latitude of Austin and Ely in Nevada with maximum depositional ages (MDAs) ranging from 36 to 24 Ma at the top of the Titus Canyon Formation. Carbonate clasts and ash-rich horizons become more prevalent in the overlying conglomeratic Panuga Formation (which contains a previously dated 15.7 Ma ash-flow

*Current address: Stanford Law School, 559 Nathan Abbott Way, Stanford, California 94305-8610, USA.
†Current address: Geosciences and Environmental Change Science Center, U.S. Geological Survey, P.O. Box 25046, MS 980, Denver, Colorado 80225-0046, USA.

tuff). The base of the higher, ash-dominated Wahguyhe Formation yielded a MDA of 14.4 Ma. The central Funeral Mountains section exposes a different sequence of units that, based on new data, are correlative to the Titus Canyon, Panuga, and Wahguyhe Formations at locations 1 and 2. An ash-flow tuff above its (unexposed) base provided a MDA of 34 Ma, and the youngest sample yielded a MDA of 12.7 Ma. The striking differences between age-correlative sections, together with map-based evidence for channelization, indicate that the Titus Canyon Formation and overlying units likely represent fluvial channel, floodplain, and lacustrine deposits as sediments mostly bypassed the region, moving south toward the Paleogene shoreline in the Mojave Desert. The profound changes in source regions and sedimentary facies documented in the Titus Canyon Formation took place during ignimbrite flareup magmatism and a proposed eastward shift of the continental divide from the axis of the Cretaceous arc to a new divide in central Nevada in response to thermal uplift and addition of magma to the crust. This uplift initiated south-flowing fluvial systems that supplied sediments to the Titus Canyon Formation and higher units.

INTRODUCTION

Mesozoic crustal thickening in the Sevier fold-and-thrust belt is widely thought to have produced a high plateau called the "Nevadaplano" across the region of the present-day Great Basin (Fig. 1), a concept introduced by DeCelles (2004). Although the idea of the Nevadaplano is broadly accepted, there is disagreement regarding the exact time and cause of plateau uplift (cf. Parsons et al., 1994; Mix et al., 2011; Cassel et al., 2018), its peak elevations (cf. Chase et al., 1998; Wolfe et al., 1998; Best et al., 2009), and if and when it experienced gravity-driven "collapse" (e.g., Sonder et al., 1987; McQuarrie and Chase, 2000; Colgan and Henry, 2009; Colgan et al., 2010; Long, 2012; Wells et al., 2012; Lee et al., 2017). There is also uncertainty about the internal topography of this inferred plateau after magmatism ended in the Sierran arc ca. 85 Ma and thrust faulting waned in the Sevier belt, which formed the eastern side of the proposed plateau (Fig. 1). There is general agreement that the region's topography was significantly flatter and featureless after Eocene to Miocene ignimbrite flareup magmatism. This inference is based on the widespread development and persistence of a subvolcanic unconformity as well as overlying volcanic rocks that blanketed the entire region without significant erosion until Miocene Basin and Range faulting began (e.g., Van Buer et al., 2009).

A curious aspect of the Nevadaplano is that the retro-arc region of the southern extent of the Sevier fold-and-thrust belt near Las Vegas (Fig. 1) lay at or near sea level by the latest Cretaceous to Paleocene, despite sharing a similar history of crustal thickening with its counterpart to the north in Utah-Wyoming (Fig. 1). This is indicated by the presence of marine fossils in Paleocene strata in the El Paso Mountains, California (Cox, 1982; Cox and Diggles, 1986; Lofgren et al., 2008). The lower elevations in the south have been explained by extensional thinning of Cretaceous arc crust during Laramide shallow slab subduction (e.g., Saleeby et al., 2007). Stable isotope data and detrital zircon age distributions from sedimentary rocks demonstrate the low-lying nature of the southernmost part of the batholith

and point to source regions in the northern part of the batholith, where sediment was transported to the southernmost Sierra Nevada region between latest Cretaceous and Eocene time by south-flowing river systems (Lechler and Niemi, 2011; Lechler et al., 2013). Consequently, at least by this time, the southern edge of the hypothesized Nevadaplano must have been located some distance to the north of exposures of marine strata, limiting its possible geographic extent (Lechler and Niemi, 2011).

Another fundamental question about the Nevadaplano concerns the nature of its topography and location of its crest over time. One view was presented by Van Buer et al. (2009), who restored the Cenozoic volcanic unconformity across the Sierra Nevada and Great Basin, creating a regional sub-unconformity geologic map. Their analysis showed several more kilometers of erosion within the arc than in areas in the retro-arc region to the east. Based on this relationship, they reasoned that the Late Cretaceous continental divide likely lay along the axis of the Cretaceous arc. This inference is supported by a lack of debris derived from the retro-arc region in the sedimentary fill of the Great Valley until later in the Eocene (Sharman et al., 2015). In another view, the pattern and age of Cenozoic ash-flow tuffs that filled mapped paleovalley channels beneath the Cenozoic volcanic unconformity are thought to define a clear N-S–trending crest for the continental divide through central Nevada (Fig. 2; e.g., Henry, 2008; Best et al., 2013; Henry and John, 2013), which is often assumed to represent the divide during the Late Cretaceous as well (e.g., Cassel et al., 2009; Henry et al., 2012).

Here, we addressed these questions with a study of channelized fluvial deposits in the Death Valley area that include the Eocene–Oligocene Titus Canyon Formation, its overlying units, and their correlatives, which together provide a new record of regional topographic development and paleogeography of the Great Basin region prior to Basin and Range faulting. The Titus Canyon Formation was previously interpreted to have been deposited within a normal fault–bounded basin, supporting suggestions that extension began early in Death Valley, prior to and during its deposition (e.g., Reynolds, 1969; Saylor, 1991; Snow

and Lux, 1999; Niemi, 2002). Fridrich and Thompson (2011) alternatively suggested that strata of this age represent fluvial sediment bypass through the region, prior to the onset of extension. This more recent interpretation by Fridrich and Thompson (2011) is supported by the new data discussed here. These new data reveal that the sources of sediment to the Death Valley region changed during the Eocene (between ca. 38–37 and at or slightly after 36 Ma), from sources that included the Mesozoic batholith to extraregional sources derived from caldera complexes and their outflow sheets that erupted across northern and central Nevada at the latitude of Austin and Ely (Figs. 1 and 2). The new data support the conclusions by Lund Snee and Miller (this volume), who propose that the evolving paleogeography

and topography of the Great Basin portion of the Nevadaplano were linked to the southward sweep of magmatism from Eocene to Miocene time. As volcanism migrated southward, thermal and magmatic input into the underlying crust supported dynamic highlands that modified the Late Cretaceous paleogeography of the inferred Nevadaplano.

GEOLOGIC BACKGROUND AND SETTING

Strata of the Titus Canyon Formation and overlying units are discontinuously exposed from the southeastern Funeral Mountains to the northeastern flanks of the Funeral Mountains and the adjacent Grapevine Mountains of the Death Valley region (Fig.
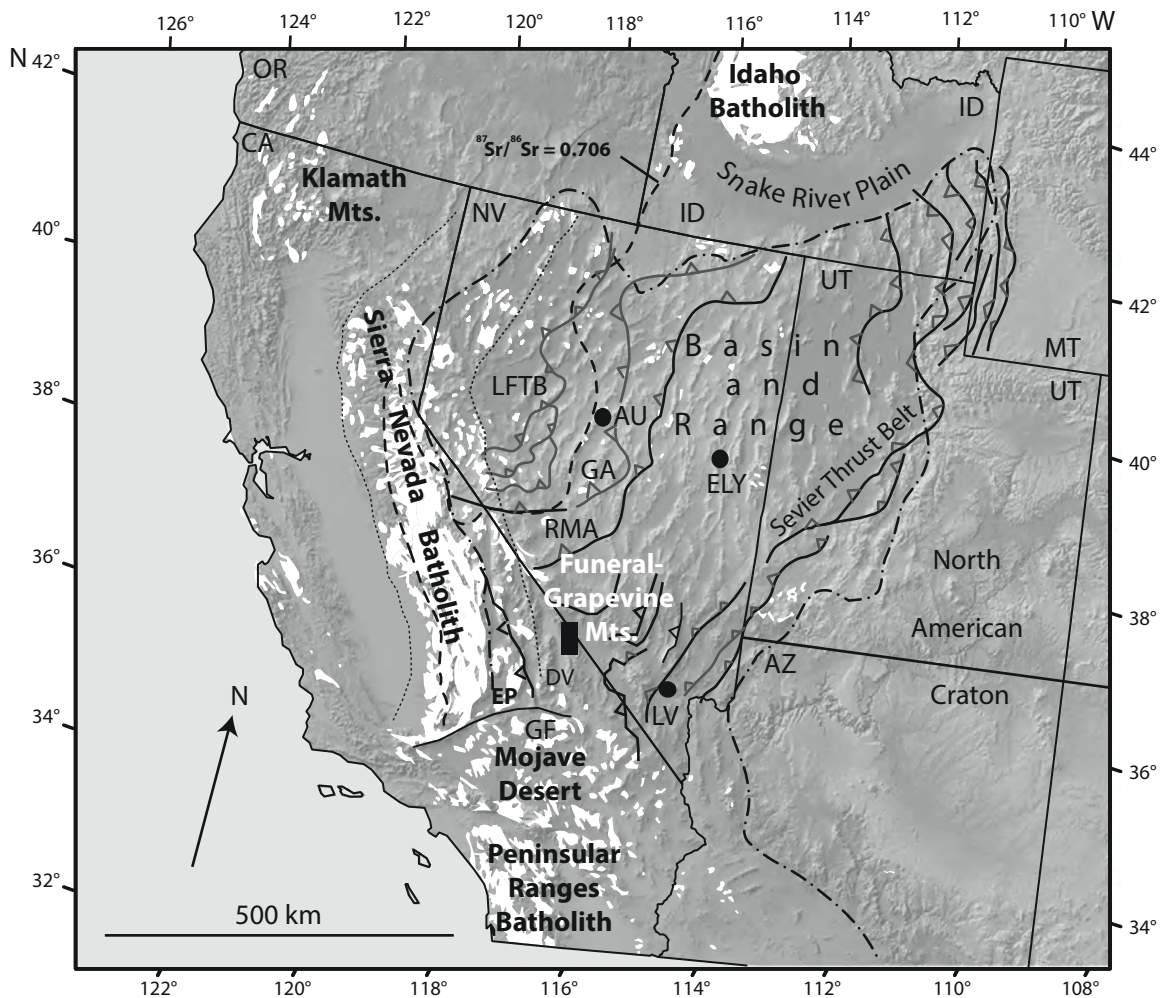

Figure 1. Index map showing the location of the study area (small black box) with respect to igneous rocks of the Mesozoic magmatic arc (white) after Van Buer and Miller (2010). Dashed black line follows the $^{87}Sr/^{86}Sr = 706$ line of Farmer and DePaolo (1983). Dash-dot line outlines the Basin and Range province. Dotted lines include the main axis of the Cretaceous part of the Mesozoic Sierra Nevada batholith. RMA are rocks of the lower Paleozoic Roberts Mountains allochthon, while GA are rocks of the upper Paleozoic Golconda allochthon. LFTB is the location of the Mesozoic Luning Fencemaker thrust belt after Oldow (1984). The location of the Mesozoic Sevier thrust belt is after DeCelles (2004). EP—El Paso Mountains, north of the Garlock fault (GF). DV—Death Valley; LV—Las Vegas; AU—Austin, Nevada. State abbreviations: CA—California; OR—Oregon; NV—Nevada; ID—Idaho; MT—Montana; UT—Utah; AZ—Arizona.

3). These deposits are cut by multiple normal faults and by the Miocene Boundary Canyon detachment and associated faults. The results of this preliminary study form part of a broader, ongoing mapping project focused on more accurately determining the Miocene offset and slip history of the Boundary Canyon detachment fault. As we mapped portions of the Boundary Canyon fault and the Cenozoic units offset by it, we identified clast types in the Titus Canyon Formation that appeared to have been derived from the erosion of the Golconda and Roberts Mountains allochthons exposed across northern Nevada, an observation that had not been previously made. Recognition of these clast types led to this study of the detrital zircon geochronology of the Titus Can-
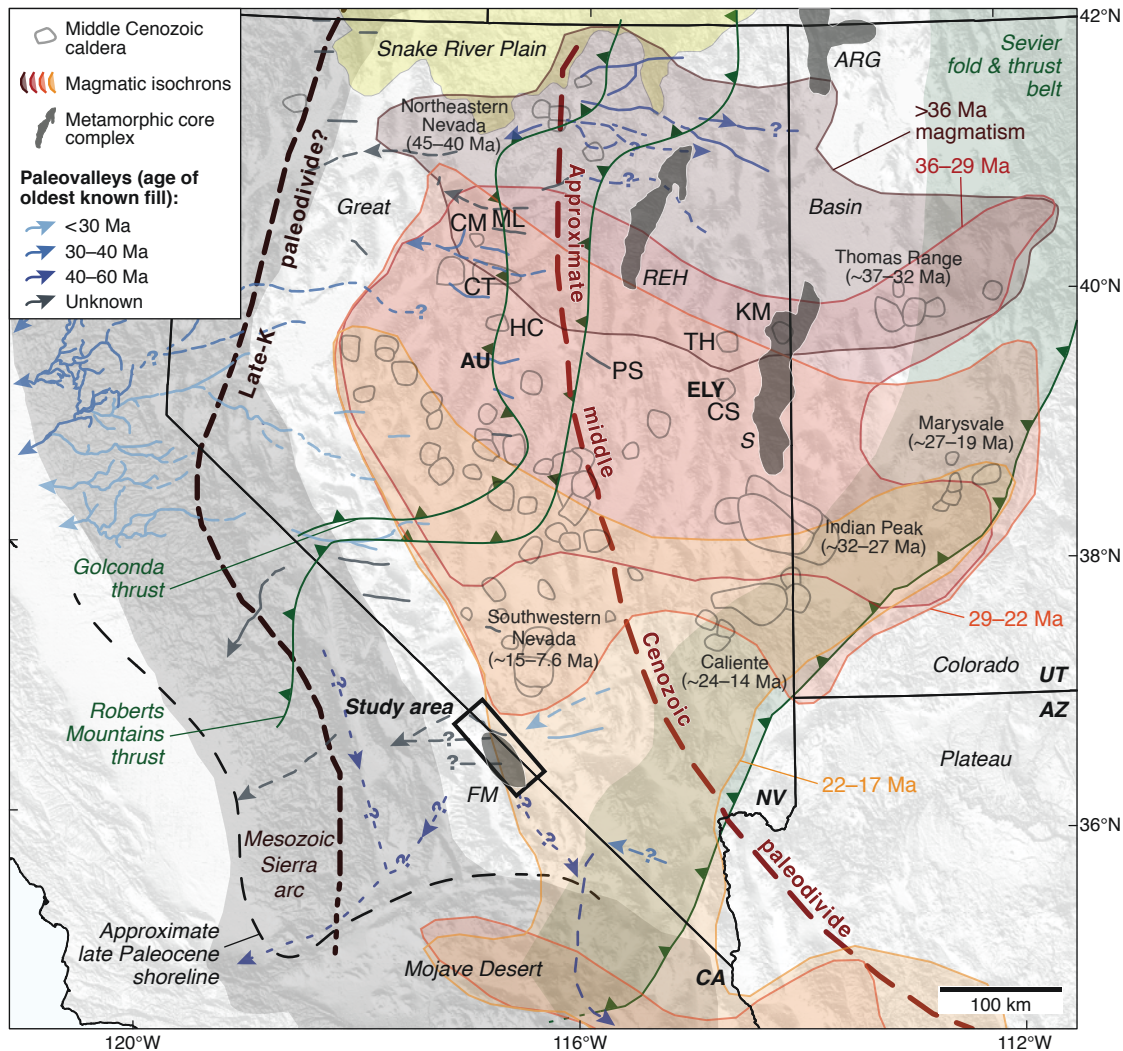
Figure 2. Map of the Great Basin, including the area presumed to have formed the Nevadaplano (DeCelles, 2004). The approximate late Paleocene ocean shoreline is after Reid (1988) and Lechler and Niemi (2011). The inferred Late Cretaceous (Late-K) continental divide is shown along the axis of the Cretaceous arc (dark red dashed line). The bright red dashed line shows the continental divide inferred from Eocene–Oligocene paleochannels from Henry et al. (2012). Source calderas for these tuffs (outlined round areas) have been largely identified (Henry and John, 2013). Volcanic isochrons, based on volcanic ages from the North American Volcanic and Intrusive Rock Database (NAVDAT; http://ecp.iedadata.org), show the southward migration of Cenozoic magmatism. Eastern extents of the Roberts Mountains and Golconda allochthons are from DeCelles (2004). Specific calderas and outflow deposits that are likely sources for zircons in the lower part of the Titus Canyon Formation (from Henry and John, 2013) are shown by the initials of their deposits: PS—Pancake Summit Tuff (35.5 Ma); CS—tuff of Cooper Summit (35.7 Ma); ML—tuff of Mount Lewis (35.81 ± 0.29 Ma); TH—tuff of Hunter District (36.1 Ma); HC—tuff of Hall Creek (33.92 ± 0.02); CT—Caetano Tuff (34.00 ± 0.05 Ma); CM—tuff of Cove Mine (34.4 ± 0.02 Ma); KM—Kalamazoo volcanics (35 Ma); REH—Ruby Mountains–East Humboldt Range metamorphic core complex; ARG—Albion–Raft River–Grouse Creek Mountains; AU—Austin; FM—Funeral Mountains; S—Snake Range. See Figure 1 for state abbreviations.
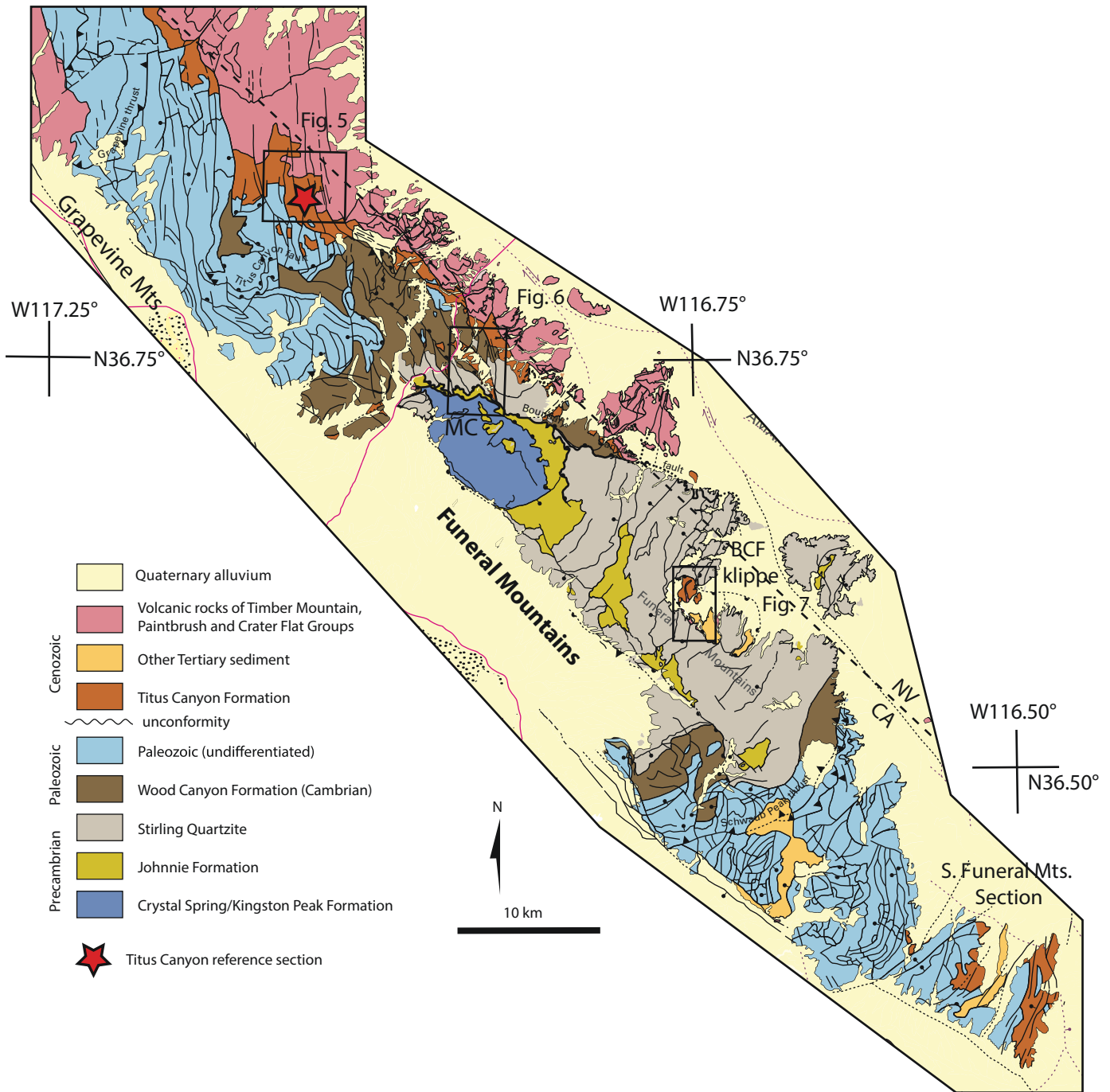
Figure 3. Index geologic map of the Funeral and Grapevine Mountains, Death Valley, Nevada-California, after Workman et al. (2002). Mesozoic thrust faults are shown by triangles with teeth pointing toward upper plate; low-angle normal faults are shown by half circles; and high-angle normal faults are shown with a single ball on the hanging wall and include smaller-offset faults with no decoration. MC—Monarch Canyon; BCF—Boundary Canyon fault. Square outlines are approximate locations of maps showing sample locations in Figures 5, 6, and 7. Exposures of age-equivalent units noted in the southernmost Funeral Mountains were mapped and described by Fridrich et al. (2012).

yon Formation in order to help us understand the paleogeography and topographic evolution of the western United States and the changing nature of the Nevadaplano.

Here, we briefly describe the geologic setting of the exposures of the Titus Canyon Formation and their structural relation with respect to the Boundary Canyon fault (Figs. 3 and 4). In the southeastern Funeral Mountains, Titus Canyon–equivalent and associated younger units unconformably overlie Devonian carbonate rocks, are cut and repeated by northwest-dipping normal faults, and have been moderately to steeply tilted to the southeast. They were mapped and described in detail by Fridrich et al. (2012) and Fridrich and Thompson (2011) and are inferred to lie in the footwall of the Boundary Canyon fault (Figs. 3 and 4). The next exposures of Cenozoic strata (studied in this contribution) were mapped by Wright and Troxel (1993) and Raftrey (2020) and lie within a klippe of the Boundary Canyon fault in the central Funeral Mountains (Fig. 3). Wright and Troxel (1993) did not specifically correlate them to the Titus Canyon Formation or higher units in the Titus Canyon type section. The base of the Cenozoic stratigraphic section in the klippe is not exposed, but it is inferred to unconformably overlie the Neoproterozoic Stirling Quartzite (Fig. 4; Raftrey, 2020). Strata dip steeply and are truncated below by the Boundary Canyon fault.

Additional sections of the Titus Canyon Formation and overlying units are exposed across a broad region east and north of the headwaters of Monarch Canyon (Figs. 3 and 4), where they dip moderately to steeply and are cut and repeated by faults within the upper plate of the Boundary Canyon fault. The exposures sampled in these areas were previously mapped by Saylor (1991) and Wright and Troxel (1993). North of Monarch Canyon, the Boundary Canyon fault dips beneath the Grapevine Mountains (Fig. 3).

The Titus Canyon Formation and overlying units (Fig. 4) are best exposed and most accessible in the Grapevine Mountains, where their type area lies in the headwaters of Titus Canyon (Fig. 3). There, these deposits rest depositionally on Cambrian strata and consist of a somewhat faulted, but generally intact, ~1000-m-thick succession of clastic strata (Fig. 4). Cenozoic strata there were first described by Stock and Bode (1935), who estimated an early Oligocene age for the Titus Canyon Formation based on titanothere, horse, rhinoceros, artiodactyl, and scinromorph fossils in the lower part of the formation. Reynolds (1969) established a reference section for the Titus Canyon Formation north of The Narrows on the east side of Titus Canyon (Fig. 3). His subdivisions are informal and were not confirmed outside of the measured sections. The stratigraphy of the Titus Canyon Formation was further described by Cornwall and Kleinhampl (1964), Hunt and Mabey (1966), Saylor (1991), and Niemi (2002). Snow and Lux (1999) revised the unit descriptions in the Grapevine Mountains, and these were again revised by Niemi (2002). Fridrich and Thompson (2011) gave a regional and in-depth overview of the Cenozoic stratigraphy of Death Valley and surrounding regions, including the Titus Canyon Formation. A detailed description of the fossil localities and their positions

in this section was recently completed by Lander (2019), who assigned them a late middle Eocene age, ca. 38–37 Ma.

For the geologic map showing sample localities (Fig. 5) and the highly simplified stratigraphic column of the Titus Canyon reference section (Fig. 4), we employed Niemi's (2002, 2012) local unit designations and geologic mapping. Niemi (2002, 2012), following Reynolds (1969), summarized the Titus Canyon Formation in its type area as containing locally derived monolithic breccia deposits at its base (derived mostly from rocks immediately underlying the basal unconformity) overlain by a variegated facies of predominantly pebble to cobble conglomerates and sandstone, along with lesser calcareous siltstones, mudstones, and marls (Fig. 4). Snow and Lux (1999) and Niemi (2002) assigned overlying strata to the Panuga Formation (Fig. 4). The Panuga Formation was originally included as part of the Titus Canyon Formation (Stock and Bode, 1935; Reynolds, 1969) and referred to as the green conglomerate facies. This subdivision was based on the recognition of an unconformity between it and the underlying Titus Canyon Formation, as well as a marked increase in volcanic material in the overlying Panuga Formation. Cobbles, like those in the conglomerates of the underlying Titus Canyon Formation, are mostly well rounded, but more angular limestone cobbles are increasingly present up section in the Panuga Formation. Pebbles of rhyolite and welded tuff also increase in abundance up section, and their prevalence is diagnostic of the Panuga Formation, as is a greater ash component to the sediments. Above the Panuga Formation, there is an ~500–850-m-thick succession of reworked ash-rich sandstones, shales, and conglomerates referred to as the Wahguyhe Formation by Niemi (2002, 2012) (Fig. 4). Above these units, there lies a thick series of ignimbrites and lavas erupted from the Southern Nevada volcanic field (Fig. 2), which range in age from ca. 14 to ca. 11 Ma. These volcanic rocks are in turn overlain by more local eruptive units spanning ca. 10.6 Ma to the present (Niemi, 2002; Fridrich and Thompson, 2011).

METHODS

The geologic map portions presented here (Figs. 5, 6, and 7) provide detailed geologic and stratigraphic context for the samples we collected, so that future workers can better utilize

Figure 4. Comparative stratigraphic columns of Cenozoic sedimentary sections with a summary of detrital zircon ages younger than 300 Ma from this study. Section locations are shown in Figure 3. For description of full detrital zircon age distributions and calculations of maximum depositional ages (MDAs, summarized here), see Supplemental Data Table S1 and Appendix S1 (see text footnote 1). Stratigraphic column from the southernmost Funeral Mountains was compiled from Fridrich et al. (2012) and employs their unit abbreviations. Thicknesses and rock types shown are respectively approximate and generalized. TCF—Titus Canyon Formation; BCF—Boundary Canyon fault; Pz—Paleozoic.
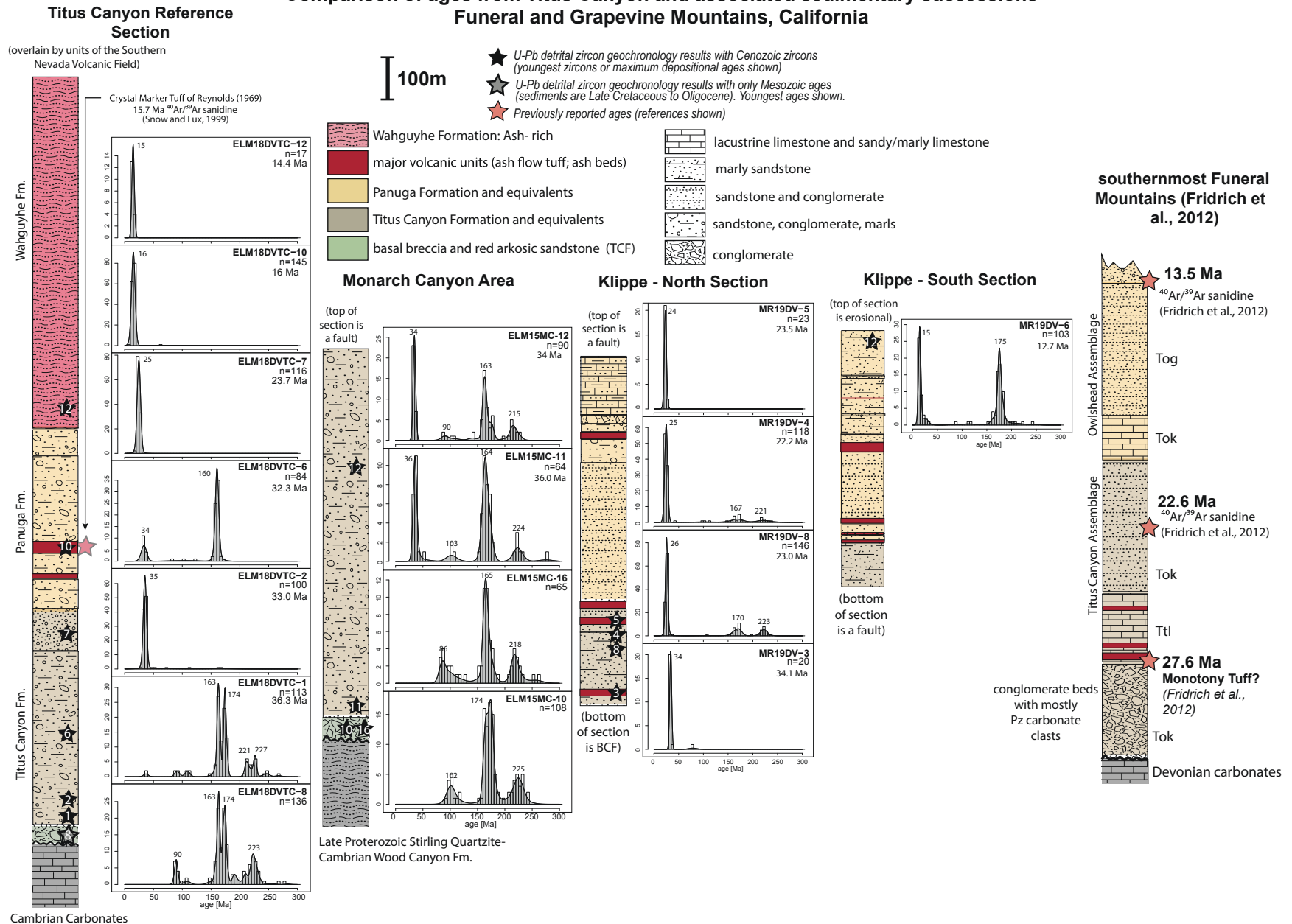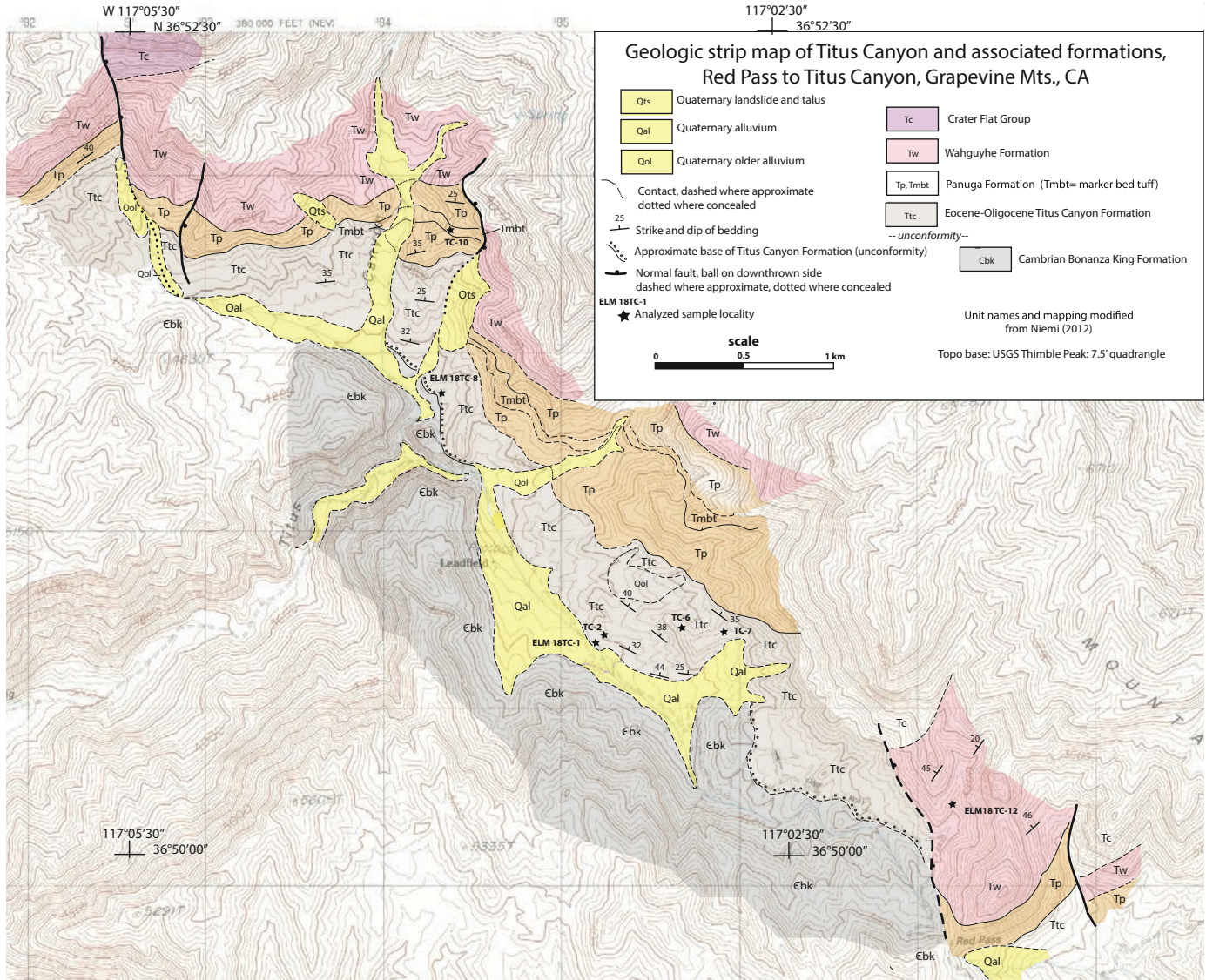
Figure 4.

Figure 5. Geologic map showing locations of analyzed samples in the Titus Canyon area, Grapevine Mountains, California. See Figure 3 for map location. Unit names and geologic mapping are modified from Niemi (2002, 2012). (Base map: U.S. Geological Survey, 1988c.)

and build on the preliminary data presented here. Sample locality coordinates and basic rock types sampled are listed in Table 1. We were able to use the stratigraphic definitions of the Titus Canyon Formation from its reference section (Niemi, 2002) in its exposures at the headwaters of Monarch Canyon (Fig. 6), where the base of the section is also well exposed. Cenozoic strata in the upper plate of the Boundary Canyon fault klippe in the central Funeral Mountains previously mapped by Wright and Troxel (1993) were mapped in greater detail by Raftrey (2020), and the new mapping is presented here (Fig. 7). In that section, we were unable to use the unit designations from the type area of the Titus Canyon Formation. For that reason, and because the ages of these units were previously so poorly known, the geologic map of the Boundary Canyon fault klippe (Fig. 7) utilizes lithologic

designations. All three maps show the new detrital zircon sample localities and provide the geologic context for the generalized stratigraphic columns shown in Figure 4.

Detrital zircon samples were processed using standard zircon separation techniques involving crushing, grinding, Gemini water table concentration of high-density components, magnetic separation, and heavy liquids density separation. Concentrated zircon separates were mounted at the University of Arizona Department of Geosciences LaserChron Center. Mounted separates were photographed on a scanning electron microscope (SEM) using backscatter electron (BSE) imaging for zircon identification. The primary standard for all samples was Sri Lanka (SL) zircon (563 ± 3.2 Ma ^{206}Pb/^{238}U age from Gehrels et al., 2008). Samples were run in two sessions on a Nu Plasma HR
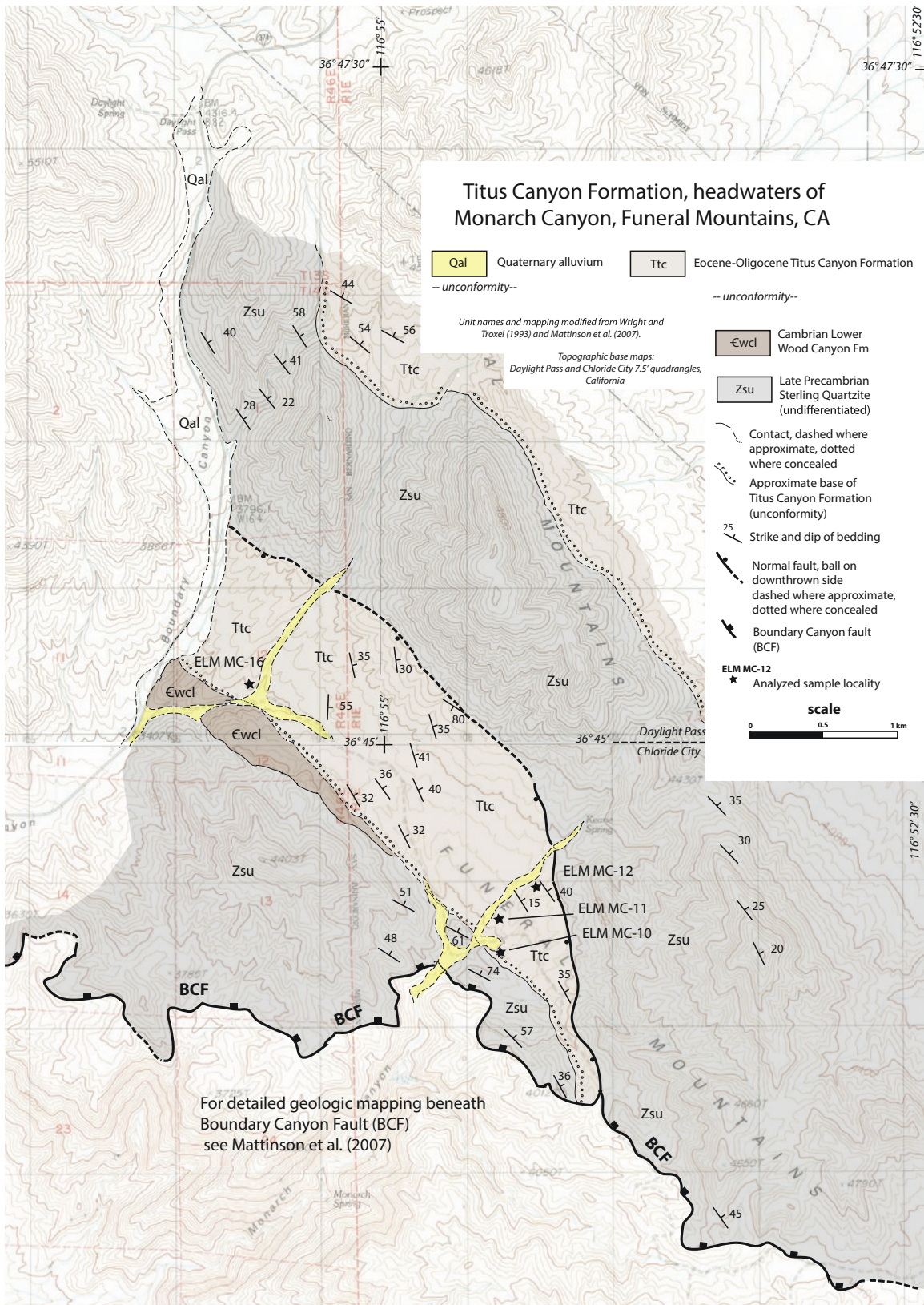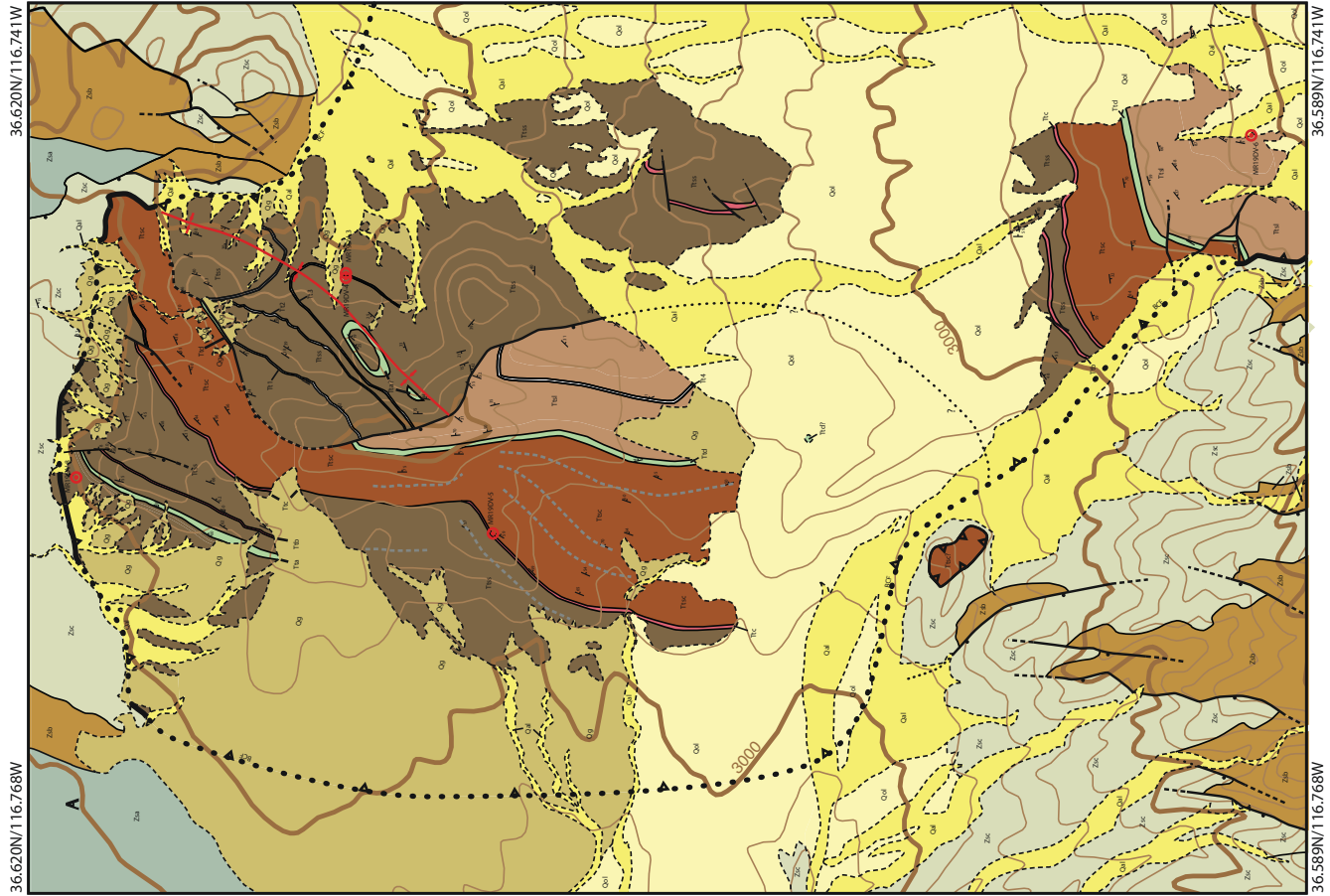
Figure 6. Geologic map showing locations of analyzed samples in the headwaters of Monarch Canyon, northern Funeral Mountains, California. See Figure 3 for map location. Unit names and geologic mapping are modified from Wright and Troxel (1993) and Mattinson et al. (2007). (Base maps: U.S. Geological Survey, 1988a, 1988b.)

Map units

Qal Alluvium (Quaternary)

Qg Younger gravels (Quaternary)

unconformity

Qol Older alluvium

unconformity

Ttsl Lacustrine siltstone, limestone and tuff (air fall tuff Tt4 shown in white)

Ttd Ash flow tuff "d" – Green-tan crystal-rich ash flow tuff

Ttsc Titus Canyon Formation - Massive siltstone, sandstone and conglomerate

Ttss Titus Canyon Formation - Interbedded tuff, siltstone, sandstone and limestone (ash flow tuffs Tta in green, Ttb/Ttc in pink; air fall tuffs Tt1,Tt2,Tt3 in white)

Cenozoic

Boundary Canyon fault

Zsc Stirling Quartzite member C (dolomite and limestone)

Zsb Stirling Quartzite member B (interbedded quartzite, siltstone and dolomite)

Zsa Stirling Quartzite member A (quartzite with minor siltstone)

Neoproterozoic

Map symbols

— · · ? lithologic conact. Dashed where inferred, dotted where concealed, queried where uncertain

— · · ? normal fault conact. Dashed where inferred, dotted where concealed, queried where uncertain, ball on downthrown side

syncline, dashed where inferred

60 strike and dip of bedding

● analyzed sample location

N

1 km

contour interval 40'

Figure 7. Geologic map showing locations of analyzed samples in the Boundary Canyon fault klippe, central Funeral Mountains, California. See Figure 3 for map location. Geologic mapping is from Raftrey (2020). BCF—Boundary Canyon fault.

TABLE 1. SAMPLE LOCALITIES ANALYZED IN THE GRAPEVINE AND FUNERAL MOUNTAINS, CALIFORNIA

Sample no.	Latitude* (°N)	Longitude* (°W)	General location	Formation	Lithology
ELM18DVTC-1	36.843966	117.05466	Titus Canyon type section	Titus Canyon	Sandstone
ELM18DVTC-2	36.844193	117.05427	Titus Canyon type section	Titus Canyon	Sandstone
ELM18DVTC-6	36.84493	117.05031	Titus Canyon type section	Titus Canyon	Sandstone
ELM18DVTC-7	36.844348	117.04692	Titus Canyon type section	Titus Canyon	Marly sandstone
ELM18DVTC-8	36.856294	117.0649	Titus Canyon type section	Titus Canyon	Red sandstone
ELM18DVTC-10	36.864494	117.0645	Titus Canyon type section	Panuga Fm	Ash-flow tuff
ELM18DVTC-12	36.836138	117.03222	Titus Canyon type section	Wahguyhe Fm.	Ash-rich marl
ELM15MC-10	36.737566	116.90989	Monarch Canyon headwaters	Titus Canyon	Red sandstone
ELM15MC-11	36.739036	116.90889	Monarch Canyon headwaters	Titus Canyon	Sandstone
ELM15MC-12	36.741279	116.90561	Monarch Canyon headwaters	Titus Canyon	Marly sandstone
ELM15MC-16	36.754876	116.92818	Monarch Canyon headwaters	Titus Canyon	Sandstone
MR19DV-3	36.612084	116.74935	Central Funeral Mountains klippe	Unknown	Ash bed
MR19DV-4	36.612085	116.74947	Central Funeral Mountains klippe	Unknown	Sandstone
MR19DV-5	36.608346	116.75752	Central Funeral Mountains klippe	Unknown	Ash-flow tuff
MR19DV-6	36.589522	116.74506	Central Funeral Mountains klippe	Unknown	Sandstone
MR19DV-8	36.618763	116.7556	Central Funeral Mountains klippe	Unknown	Sandstone
*World Geodetic System 1984 (WGS84).					

multicollector–inductively coupled plasma–mass spectrometer outfitted with a Photon Machines G2 excimer laser following the methods of Gehrels et al. (2008) and Gehrels and Pecha (2014). Between 100 and 150 zircon grains were analyzed from detrital zircon samples, and ~25 zircons were analyzed from volcanic samples. All analyses employed a 30 μm laser spot size. Grains were selected for analysis by a random walk transect across the BSE images. Data reduction for the first set of analyses was done using the LaserChron AgeCalc program for Microsoft Excel. Data from the second session were reduced using the AgeCalcML program of Sundell (2019). Kernel density estimate plots were created using the IsoplotR program of Vermeesch (2018). A ^{204}Pb-based common Pb correction was applied to all analyses. The ^{206}Pb/^{238}U ages are reported for grains up to 900 Ma, and ^{207}Pb/^{206}Pb ages are reported for older grains. The ^{206}Pb/^{238}U ages with errors >10% were filtered from the data set, and ages older than 600 Ma were filtered based on 20% discordance or greater than 10% reverse discordance. Analytical data can be found in Supplemental Data Table S1[1] and include only the results used in the subsequent analysis. Our analysis of the data focused primarily on the age of Cenozoic zircon grains and on the switch from sandstones with Mesozoic-age zircons to those with dominantly Cenozoic zircons. Because this was a reconnaissance study, further work on the detailed stratigraphic context of the samples as well as more detailed sampling and analysis will certainly add to the results presented here.

A benefit of measuring detrital zircon U-Pb age distributions is that results can be used to place a maximum bound upon the depositional age of the sample, following Dickinson and Gehrels (2009) and Gehrels (2013). Various statistical methods can be applied to systematically calculate the maximum depositional age (MDA) for a detrital zircon sample, but none of these guarantees that a MDA will approximate the true depositional age of a sample, because the youngest grains could be far older than the age of deposition of their host rocks (e.g., Coutts et al., 2019). From a general geologic perspective, however, volcanism was semicontinuous from the Eocene to the present-day across much of what was to become the Basin and Range Province (Fig. 2), so that the chance of sediments deposited during that age span being much younger than their youngest included zircons is likely small, but possible. In most cases, the weighted mean of a small set of young grains overlapping in age within 1σ error (YC1σ) is reported as the MDA. The grains selected for estimating each MDA were chosen such that grain ages overlapped within 1σ error of each other, they formed a discrete cluster of ages distinct from the rest of the young ages, and they did not have high U (an indicator of possible radiation damage and consequent Pb loss). Further evaluation of a given set of young ages to determine whether they represented a discrete group came from their U/Th ratios, which can be affected by crustal heritage or interaction with metamorphic fluids. If the U/Th ratios of grains forming the YC1σ group are appreciably different from those of the rest of the young ages, this supports the interpretation of them as a discrete group and the ability to use their weighted mean as the MDA for the sample. In cases where there is no set of overlapping young ages, the youngest single grain (YSG) from a set of detrital zircon ages was used as an estimate of the MDA (see

Dickinson and Gehrels, 2009). We emphasize that the YSG age is the least reliable of the methods used here, and it was only used where the youngest single grain did not have high U, which is a measure of potential radiation damage and thus Pb loss. The Supplemental Data Appendix S1 describes in more detail each of the samples analyzed and illustrates the basis for determination of the MDAs (Figs. S1–S6) that are listed in the stratigraphic columns of Figure 4.

RESULTS

Observations Based on Regional Relations and Geologic Mapping

Mapping of Cenozoic units in the Funeral Mountains formed part of a broader ongoing effort to determine the Miocene offset and slip history along the Boundary Canyon fault. We emphasize that much more detailed sedimentologic and stratigraphic work is needed on Cenozoic units and specifically the Titus Canyon Formation to fully understand its age and how its different sections correlate to one another. However, our local mapping of sedimentary successions and the faults that cut them revealed several important insights. Based on the map-scale and outcrop unit geometries and the varied nature and thicknesses of successions present in the various areas studied (e.g., Figs. 5, 6, and 7), we found that lateral variations (in terms of lithology and thicknesses) are pronounced within the Titus Canyon Formation, overlying units, and their equivalents (Fig. 4), even at the scale of individual outcrops. Within these successions, we observed truncations of stratigraphy and changes in thickness and lithology, together providing evidence for fluvial incision of younger beds into underlying strata. As discussed in more detail below, there is variability in the ages represented by the different mapped sections, as well as a lack of correspondence of stratigraphic units and interbedded volcanic horizons between these sections (Fig. 4).

These relationships and the variable succession of rock types portrayed in Figure 4 suggest that the Titus Canyon Formation, its overlying units, and their equivalents were likely deposited by numerous migrating fluvial channels that interfingered laterally with floodplain and lacustrine environments. In such a depositional environment, it would be common to channelize, erode, and rework older deposits. This depositional framework would also help to explain why distinctive (but different) volcanic horizons are present in several of the sections (Fig. 4). Volcanic units, such as ignimbrites, might be restricted to the channels that were active at a given time, and each preserved channel-fill succession might include a different set of units and volcanic horizons. Although additional sedimentologic and stratigraphic analysis is still needed to fully characterize the depositional setting of the Titus Canyon Formation and its overlying units and equivalents, our observations are consistent with those of Fridrich and Thompson (2011), who suggested that the channelized deposits represent less depositional accumulation and more sedimentary bypass or transport through the region rather than the sedimentary filling of a locally fault-bounded basin. Based on geologic mapping and the study of the units at a regional scale, Fridrich and Thompson (2011) pointed out that a defining feature of the clastic part of the succession is the distal provenance for these predominantly fluvial strata. Based on the nature and distribution of mapped fluvial successions, they also inferred that they were deposited across a broad region and predated Basin and Range faulting (Fridrich and Thompson, 2011). They also noted the ash component of the siltstones, shales, and marls and concluded that it reflected a northern source because volcanism only arrived in the Death Valley region after Eocene–Oligocene time (Fig. 2). Finally, they noted the up-section increase in abundance of intercalated volcanic material and suggested that it likely reflected the progressive advance of active volcanism, from north to south, into the region between 40 and 19 Ma.

Detrital Zircon Geochronology Results: Titus Canyon Type Section and Headwaters of Monarch Canyon

Here, we report the results of detrital zircon analyses from 11 samples from the Titus Canyon Formation, its overlying units in the Titus Canyon reference section, and its equivalents in the Monarch Canyon area (Figs. 3–6).

Three samples collected from the base of the section near Titus Canyon and the headwaters of Monarch Canyon were analyzed for U-Pb detrital zircon ages (Fig. 4, Titus Canyon reference section and Monarch Canyon area columns; sample localities are listed in Table 1 and are shown on Figures 5 and 6). These samples were collected from thin (a few meters thick) sections of red arkosic sandstone just above coarse conglomerate and breccias, which usually characterize the base of the Titus Canyon Formation (Reynolds, 1969; Niemi, 2002). These included sample ELM18DVTC-8 in the type section and samples ELM15MC-10 and ELM15MC-16 from the section at the headwaters of Monarch Canyon (Figs. 4, 5, and 6). These three samples contained detrital zircon distributions that are almost entirely Mesozoic in age, including Triassic, Jurassic, and Cretaceous peaks, and only sparse older grains (Fig. 4). The stratigraphically lowest sample collected in the Titus Canyon section (ELM18DVTC-8, $n = 147$) is a red sandstone interlayered with the top of a several-meter-thick basal sedimentary breccia at the base of the unit (Fig. S1 [see footnote 1]). The sample yielded prominent age peaks at 90 Ma, 163 Ma, 174 Ma, and 223 Ma (Fig. 4; see also Supplemental Data, Appendix S1, and Figs. S1 and S2). Proterozoic grains, which do not constitute a significant fraction of the sample ($n = 13$), lie between 1050 and 1873 Ma and exhibit minor peaks at ca. 1076, 1372, and 1780 Ma (Fig. S1). Given that this unit hosts late middle Eocene fossils that are 38–37 m.y. old (Lander, 2019), the detrital zircon data do not provide a useful depositional age constraint on these sediments. Rather, we consider the fossil age as the MDA. Thus, the fossil ages of this unit provide a MDA for overlying units. In the headwaters of Monarch Canyon, sample ELM15MC-10 ($n = 116$) was taken from red sandstone within the sedimentary breccia at the base of the formation (Figs.

4 and 6; Figs. S3 and S4). The sample showed zircon age distributions with prominent peaks at 102, 174, and 225 Ma (Fig. 4; Fig. S3). Eight Proterozoic grains yielded U-Pb ages from 1006 to 1781 Ma (Fig. S3). Sample ELM15MC-16 (*n* = 99) was collected along strike from MC-10 near the mapped unconformity at the base of the Titus Canyon Formation (Figs. 4 and 5; Fig. S3), and it yielded prominent Mesozoic age peaks at 86, 165, and 218 Ma. Paleozoic to Proterozoic grains (*n* = 34) within this sample exhibited peaks at 399, 1107, 1439, and 1777 Ma, with four older grains between 1995 and 2857 Ma (Fig. S3). The zircons in these three samples indicate the red sandstones at the base of the Titus Canyon Formation do not provide useful constraints on the age range of the basal units, for which the maximum depositional age is 38–37 Ma, the age of the fossils in this part of the formation (Lander, 2019).

The first beds of well-rounded chert pebble conglomerate and interbedded sandstones (Figs. 8A and 8B) above the red bed arkosic sandstones herald an obvious change in source region as well as an increase in coarse sediment delivery to the region. Pebbles and cobbles are well rounded, are often highly polished, and consist of fine-grained, erosionally resistant rock types like chert, quartzite, and fine-grained volcanic rocks. Despite an abundance of dark chert, occasional red chert pebbles and cobbles are conspicuous in outcrop (Fig. 8B). Radiolaria are apparent in the red chert when inspected with a hand lens, and thin sections of multiple red chert cobbles better document their presence (Fig. 8C). We also observed cobbles of black chert with pale phosphatic nodules and streaks (Fig. 8G) as well as cobbles of reworked conglomerate (Fig. 8D). In thin section, the reworked conglomerate cobbles contain radiolarian-bearing chert clasts, altered mafic volcanic rocks, and fragments of mature orthoquartzite with well-rounded but poorly sorted quartz grains (Figs. 8E and 8F). These distinctive sedimentary and igneous rock clasts are common rock types of the Lower Paleozoic Roberts Mountains and the Upper Paleozoic Golconda allochthons of Nevada (Figs. 1 and 2). For example, the black chert with phosphatic nodules (Figs. 8G and 8I) is typical of Devonian deep-water strata of the Roberts Mountains allochthon (e.g., Graber and Chafetz, 1990). The quartzite clasts in the reworked conglomerate boulders (Figs. 8D and 8E) match the distinctive well-rounded but poorly sorted quartzites of the deep-water Ordovician Valmy Formation (Fig. 8H) of the Roberts Mountains allochthon (e.g., Stewart, 1980; Miller and Larue, 1983). The combination of these distinctive quartzite clasts with radiolarian chert and mafic volcanic clasts indicates that the conglomerate could represent erosion of either the Mississippian Antler foredeep basin deposits, which were largely derived from the Roberts Mountains allochthon, or the Upper Paleozoic overlap sequence deposited across the Roberts Mountains allochthon of central and northern Nevada (e.g., Stewart, 1980; Harbaugh and Dickinson, 1981; Dickinson et al., 1983). To our knowledge, the only exposures of red radiolarian chert occur in the Upper Paleozoic Havallah sequence of the Golconda allochthon (e.g., Miller et al., 1984; Tomlinson, 1991). The combined presence of rock types that are diagnostic of the Roberts Mountains and Golconda allochthons and their associated strata strongly suggests that sediment deposited in the Titus Canyon Formation was transported to the Death Valley area from more northerly areas in the Great Basin (Figs. 1 and 2).

The stratigraphically lowest sandstones sampled for detrital zircon that are interbedded with these chert pebble conglomerate beds yielded a MDA of 36.3 Ma for sample ELM18DVTC-1 from the Titus Canyon type section and a closely matching MDA of 36.0 Ma for sample ELM15MC-11 from the Monarch Canyon area (Figs. 4, 5, and 6). Sample ELM18DVTC-1 from the Titus Canyon section was collected from coarse sandstone interbedded with conglomerate that contains abundant well-rounded black chert pebbles. Major age peaks in this sample (*n* = 116) were observed at 163 Ma and 174 Ma, with a lesser proportion of Cenozoic, Cretaceous, Triassic, and Proterozoic (1099, 1773, and 2094 Ma) zircon (Fig. 4; Supplemental Data, Appendix S1, and Figs. S1 and S2). This sample yielded only two Cenozoic grains (36.3 ± 0.2 and 37.4 ± 0.2 Ma), which did not overlap in age within error (Fig. S2). The youngest grain (36.3 ± 0.2 Ma) does not appear to have been affected by Pb loss, since it has comparable U and U/Th to that of age-equivalent zircon from other samples collected in the section, suggesting that the depositional age of ELM-18DVTC-1 is likely to have been Eocene or younger.

In the Monarch Canyon area, sandstone interbedded with the lowest horizons of chert pebble conglomerate is represented by sample ELM15MC-11 (Figs. 4 and 6). This sample (*n* = 112) contained abundant Cenozoic zircon with a peak ca. 36 Ma and Mesozoic peaks at 103 Ma, 164 Ma, and 224 Ma (Fig. 4; Fig. S3). This sample also yielded a large proportion of Paleozoic–Proterozoic grains (*n* = 48), with age peaks at 440 Ma, 1108 Ma, 1405 Ma, 1717 Ma, 1858 Ma, and 2582 Ma (Fig. S3). A group of 13 grains yielded a MDA of 35.9 ± 0.3 Ma (Fig. S4). The structurally highest sample from a marly sandstone within this exposed section (truncated above by a normal fault; Fig. 6), ELM15MC-12 (*n* = 107; Figs. 4 and 6; Fig. S3), yielded age peaks at ca. 34 Ma, 90 Ma, 163 Ma, and 215 Ma. Paleozoic–Proterozoic grains (*n* = 17) defined a peak at 1092 Ma, with additional grains between 562 Ma and 2715 Ma. The youngest 16 grains yielded a MDA of 33.61 ± 0.49 Ma (Fig. S4).

Samples from the Titus Canyon Formation in the Titus Canyon reference section that lie stratigraphically above sample ELM18DVTC-1 (Figs. 4 and 5) yielded successively younger MDAs of 33, 32, and 23.7 Ma (Fig. 4; Figs. S1 and S2). Sample ELM18DVTC-2 (*n* = 116) was collected a few meters above ELM18DVTC-1, from sandstone interbedded with chert pebble conglomerate, within the lower part of the variegated member of the Titus Canyon Formation of Reynolds (1969) (Fig. 5). Rare cobbles and pebbles of porphyritic granitoids and clasts of conglomerate were noted in adjacent conglomerates. The U-Pb age distribution of ELM18DVTC-2 was dominated by Cenozoic zircon with a few Mesozoic grains present (Fig. 4; Fig. S1). Minor Paleozoic–Proterozoic peaks were observed at 409, 1138, and 1802 Ma. The youngest grain in this sample (25.9 ± 0.1 Ma) is not considered to yield an accurate MDA based on the poor
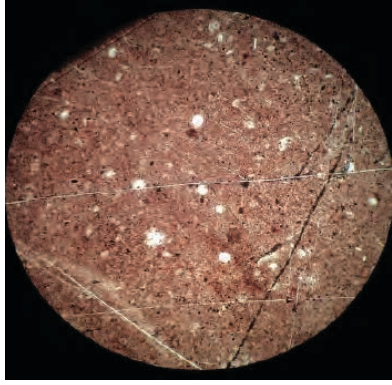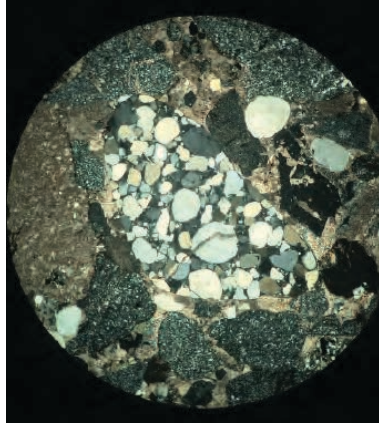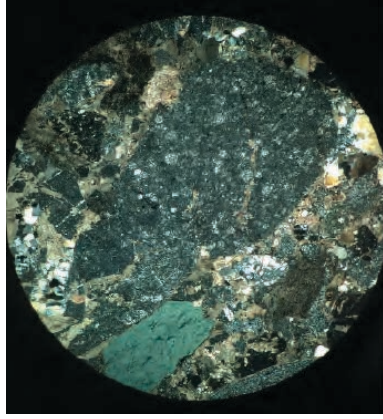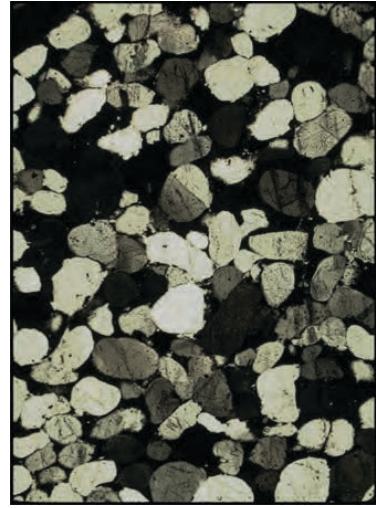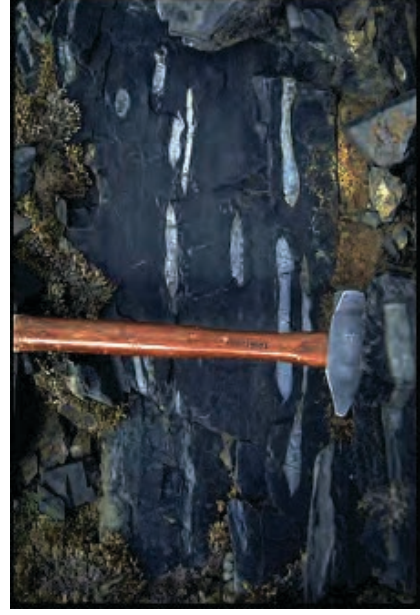
Figure 8.

quality of the analysis (i.e., high [204]Pb and low [206]Pb/[204]Pb) and a lack of additional grains of similar age (Fig. S2). However, a slightly older group of three zircon grains yielding statistically indistinguishable U-Pb ages provides an adequate basis for calculating a MDA of 33.0 ± 0.3 Ma (Fig. 4; Fig. S2).

The next sample upward in the Titus Canyon reference section, ELM18DVTC-6 ($n = 114$; Figs. 4 and 5; Fig. S1), was collected from the top of a series of coarse-grained, massive sandstone beds that are green colored in outcrop due to celadonitic alteration. The age distribution from this sample exhibited prominent Cenozoic and Mesozoic peaks at ca. 34 Ma and 160 Ma, with a few ages between these maxima (Fig. 4; Fig. S1). This sample yielded the greatest number of older grains of all samples dated in this reference Titus Canyon section ($n = 30$). These older zircons defined peaks at 478 Ma, 1085 Ma, and 1776 Ma (Fig. S1). The youngest grain from this sample was dated at 29.9 ± 0.2 Ma and did not exhibit indications of potential Pb loss (e.g., high U concentrations), but it did not overlap in age within error of any other grains. A MDA of 32.3 ± 0.3 Ma was estimated from a weighted average of two slightly older but overlapping grains that yielded identical U/Th and showed no evidence of Pb loss (Fig. S2). This MDA overlaps with the MDA of the stratigraphically lower sample ELM18DVTC-2 (Fig. 4).

ELM18DVTC-7 ($n = 116$) is the stratigraphically highest sample analyzed from the Titus Canyon Formation in the reference section (Figs. 4 and 5). The sample is a fine-grained sandstone interlayered with calcareous siltstone and laminated silty limestone that was likely deposited in a lacustrine environment. The age distribution of zircons in ELM18DVTC-7 was dominated by Cenozoic ages. The youngest single grain age of

7.0 ± 0.04 Ma was rejected based on high [204]Pb concentrations and low [206]Pb/[204]Pb (spot 110, Table S1 [see Supplemental Material]). A slightly older group of 11 grains yielded ages that all overlapped within 1σ and yielded a MDA of 23.7 ± 0.1 Ma, which we interpret to represent the preferred MDA for the sample (Fig. 4; Fig. S2).

Above this sample, there is the inferred contact between the Titus Canyon Formation and the Panuga Formation as mapped and defined by Niemi (2002, 2012). As such, the MDAs of the strata described above indicate a ca. 36–24 Ma age range for the conglomeratic part of the Titus Canyon Formation above the red beds at its base. We sampled the ash-flow tuff in the overlying Panuga Formation, called the "crystal marker tuff" by Reynolds (1969) and Niemi (2002) (Figs. 4 and 5). Snow and Lux (1999) and Niemi (2002) reported a [40]Ar/[39]Ar sanidine age of 15.7 Ma for the eruptive age of this unit. Sample ELM18DVTC-10 yielded a U-Pb age peak of ca. 16 Ma (Fig. 4; Figs. S1 and S2). Several much younger grains (10.8 Ma) are interpreted as contamination of the sample by soil particles derived from erosion of units higher in the section.

The overlying Wahguyhe Formation of Niemi (2002) in the Titus Canyon area consists of ash-rich lacustrine marls and interbedded shales that form prominent chalky white to rusty weathering exposures in the Titus Canyon area (Fig. 4). Sample ELM18DVTC-12 ($n = 17$) was collected from ash-rich strata deposited in a lacustrine environment within the basal part of the Wahguyhe Formation (Figs. 4 and 5). The 14 youngest grains from the sample yielded a weighted mean age of 14.4 ± 0.3 Ma, which we regard as a robust MDA for the sample (Fig. 4; Fig. S2). The Wahguyhe Formation is in turn overlain by ignimbrites, lava flows, and subvolcanic intrusive rocks of the Southern Nevada volcanic field that range in age from ca. 14 Ma to ca. 11 Ma (Niemi, 2002; Fridrich and Thompson, 2011; Fridrich et al., 2012).

Detrital Zircon Geochronology Results: Boundary Canyon Fault Klippe, Central Funeral Mountains

Cenozoic strata exposed within the Boundary Canyon fault–bounded klippe in the central Funeral Mountains (Figs. 3 and 7) exhibit a range of sedimentary rock types and contain intercalated ash-flow tuffs and primary and reworked ash horizons (Klippe–North Section and Klippe–South Section columns in Fig. 4). The range of rock types is similar to those present in both the Titus Canyon Formation and the Panuga Formation of the Titus Canyon area described above (Figs. 4 and 5). However, despite the similar rock types present within the klippe, the unit designations outlined by Reynolds (1969), Snow and Lux (1999), and Niemi (2002) for the Titus Canyon Formation and higher units in the Titus Canyon reference section do not directly match any part of the section of Cenozoic sedimentary rocks mapped in the klippe. Some of the mapped units here clearly truncate one another, as well as thicken and thin, suggesting deposition in channels at least hundreds of meters wide (Fig. 7).

Figure 8. (A) Outcrop photo of interbedded sands, grits, and chert pebble conglomerate (sample ELM18-DVTC-1; see Fig. 5 for location). (B) Chert pebble conglomerate near the base of the Titus Canyon Formation in Titus Canyon (Fig. 3), highlighting pebbles of red radiolarian-bearing chert. Walking pole handle (~3.8 cm) for scale. (C) Thin-section photomicrograph of red radiolarian chert. Plane light; field of view is ~5 mm across. (D) Cobbles in the Titus Canyon Formation in Titus Canyon (Fig. 3) that are composed of conglomerate with chert, quartzite, and mafic volcanic debris. (E) Thin-section photomicrograph of the conglomerate clast shown in D, containing a clast of orthoquartzite with well-rounded but poorly sorted quartz grains similar to the Ordovician Valmy Quartzite of northern Nevada, which is shown in H. Crossed-polarized light; field of view is ~5 mm across. (F) Thin-section photomicrograph of clasts in the same conglomerate depicted in D, which include dark radiolarian-bearing chert (large grain at center right) and altered mafic volcanic fragments (green grain to the upper left). Crossed-polarized light; field of view is ~5 mm across. (G) Polished clast of black radiolarian chert with phosphatic concretions. Compare to outcrop photo of Devonian chert in I. Field notebook is 11.75 cm × 17.8 cm. (H) Thin-section photomicrograph of the Ordovician Valmy Quartzite from the Roberts Mountains allochthon, Nevada (e.g., Miller and Larue, 1983). Field of view is 3.5 mm wide. (I) Outcrop photo of Devonian chert of the Roberts Mountains allochthon, Nevada, with white phosphatic concretions and streaks. Photos are by Elizabeth L. Miller.

Three sections of strata are exposed in the northern part of the Boundary Canyon fault klippe, all of which are truncated by faults and/or erosion (Fig. 7). The northern two sections form the composite section illustrated in the Klippe–North Section column of Figure 4. This composite section consists of ~100 m of conglomerate, sandstone, and ash-rich sandstone, with minor lacustrine limestone, siltstone, and ash beds (unit Ttss in Fig. 7). Its middle part, unit Ttsc, is ~200 m thick and dominated by deep red sandstone, siltstone, and conglomerate that contains an ash-flow tuff along part of its base (Fig. 7). The upper part of the section, unit Ttsl, has an exposed thickness of ~125 m and consists of light-colored yellowish siltstone interbedded with lacustrine limestone and ash-fall tuff (Fig. 7). The section is repeated by a NW-dipping normal fault, and the lowest strata in the footwall are inferred to represent the lower part of the section in the hanging wall based on the similarity of a thick water-reworked bed (unit Tta), which is folded into a gentle syncline in the footwall (Fig. 7). Both of these sections are inferred to be in normal fault contact with a section exposed farther to the southeast that also lies in the upper plate of the Boundary Canyon fault klippe (Fig. 7; see also Klippe–South Section column in Fig. 4).

Five detrital zircon samples were analyzed from the three fault-bounded sections of Cenozoic strata. Sample MR19DV-8 (*n* = 152) is a dark red-brown, coarse-grained sandstone from the structurally lowest and stratigraphically deepest exposure of strata in the northwesternmost section of the klippe (Figs. 4 and 7). This sample yielded Cenozoic–Mesozoic age peaks at 26 Ma, 170 Ma, and 223 Ma (Fig. 4; Fig. S5). Six Paleozoic grains were clustered at 419 Ma (Fig. S5). A weighted mean of three grains yielded a MDA of 23.0 ± 0.2 Ma (Fig. 4; Fig. S6). Sample MR19DV-5 (*n* = 23) was sampled from an ~4-m-thick, light pink-brown ash-flow tuff at the base of unit Ttss (Figs. 4 and 7), yielding one peak at ca. 24 Ma (Fig. 4; Fig. S5). All 23 grains intersected within error for a weighted mean age of 23.5 ± 1.1 Ma (Fig. 4; Fig. S6) that likely represents the age of this tuff. The age of the youngest single grain, which is included in this weighted mean, is 20.1 ± 3.6 Ma. The MDAs of the above two samples overlap within error.

In the footwall of the normal fault that down-drops the above section (Fig. 7), we mapped a series of ash-rich lacustrine deposits designated as units Tt1–Tt4 that lie stratigraphically beneath what might be the equivalent of Tta. The stratigraphically lowest of these tuffaceous strata, sample MR19DV-3 (*n* = 22), was collected from a white, ~2-m-thick ash bed labeled unit Tt3 on Figure 7, which was likely reworked in a lacustrine environment. This sample exhibited a prominent age peak at 34 Ma, with one Mesozoic grain and two Proterozoic grains at 1922 Ma (Fig. 4; Fig. S5). The 21 Cenozoic grains yielded a weighted mean MDA of 34.1 ± 0.5 Ma (Fig. 4; Fig. S6).

Sample MR19DV-4 was collected from an ~3-m-thick, light red-brown, calcite-cemented, coarse-grained sandstone interval stratigraphically above tuff sample MR19DV-3 of unit Tta described above. The sample yielded a prominent zircon age peak at 25 Ma (*n* = 119), with two Mesozoic grains (at 167 Ma

and 221 Ma) and only one Proterozoic grain (Fig. 4; Fig. S5). Three grains yielded a weighted mean MDA of 22.2 ± 0.2 Ma (Fig. 4; Fig. S6). It is not clear without further investigation if the juxtaposition of this relatively young sample with the underlying 34 Ma water-reworked tuff of MR19DV-3 (possibly 12 Ma older) is related to young units (e.g., represented by sample MR19DV-4) channelizing into older units (represented by sample MR19DV-3) or if sample MR19DV-3 might represent an unusual case of reworking of an exclusively older, ca. 34 Ma tuff into a possibly younger Tt3 deposit.

Sample MR19DV-6 (*n* = 126) is a light red-brown, coarse-grained sandstone that was sampled from the exposed top of the southeastern section mapped in the klippe (Fig. 4 Klippe–South Section column; Fig. 7). It represents the stratigraphically highest sample analyzed (Fig. 7). The sample yielded Cenozoic and Mesozoic peaks at ca. 15 and 175 Ma, respectively (Fig. 4; Fig. S5). Proterozoic peaks lie at 1084 Ma and 1748 Ma. Two young grains provided a weighted mean MDA of 12.7 ± 0.8 Ma (Fig. S6).

The data above suggest that the Cenozoic strata exposed in the klippe of the Boundary Canyon fault are, in part, correlative in age to the Titus Canyon and Panuga Formations in their type area, but the klippe section at its exposed top is younger than the Panuga Formation or the base of the Wahguyhe Formation (Fig. 4). Importantly, this succession of strata is tilted substantially (mostly 35°–70° but locally up to 87°) and cut by the Boundary Canyon fault, demonstrating that slip on this fault began later than 13–12 Ma.

Comparison to Southernmost Funeral Mountains Section

The Cenozoic section in the southernmost Funeral Mountains (Fig. 3; right-hand column of Fig. 4), mapped and described by Fridrich et al. (2012) and Fridrich and Thompson (2011), is considerably thicker and contains more lacustrine limestone than the sections of the Titus Canyon Formation and overlying units described above, suggesting greater sediment accumulation and preservation southward. The available age constraints for this section are shown in Figure 4 after Fridrich et al. (2012) and Fridrich and Thompson (2011). Comparison of their age constraints to the ages we obtained shows that the section in the southern Funeral Mountains is at least in part time-correlative to the Titus Canyon and Panuga Formations in their type section in Titus Canyon, as well as to the sections in the klippe of the Boundary Canyon fault (Fig. 4). However, the southernmost Funeral Mountains section, like the sections in the Boundary Canyon fault klippe, exhibits considerable differences in lithology from the previously discussed sections. Notably, the conglomerate unit at the base of the section in the southernmost Funeral Mountains (base of unit Tok of Fridrich et al., 2012) contains mostly Paleozoic carbonate clasts rather than the cobbles of typically rounded to polished chert and other resistant rock types seen in the type section of the Titus Canyon Formation (Fig. 4). The lacustrine sequences here are much thicker than those in exposures of the Titus Canyon and Panuga Formations in their type area and also form a dominant

part of the succession in the southernmost Funeral Mountains section (Fig. 4; Fridrich et al., 2012).

DISCUSSION AND CONCLUSIONS

The Titus Canyon Formation and higher units and their age correlatives described above record a fundamental change in sediment provenance in the Death Valley region. The change in provenance is tightly constrained as occurring after late middle Eocene time (38–37 Ma), based on the ages of fossils dated within the basal red beds (Lander, 2019), and by about ca. 36 Ma or slightly later, based on the oldest MDA in overlying chert pebble–bearing sandstone and conglomerate (Fig. 4). Samples from the basal red beds beneath the chert pebble conglomerates

and above the basal unconformity yielded detrital zircon suites that were mostly derived from the erosion of the broader Sierra Nevada batholith and its country rocks, for which the distribution is shown in Figure 1. Specifically, these samples (as well as the Mesozoic zircon age distributions from samples higher in the section) show well-defined peaks that closely mirror previously published age compilations from the broader Sierra Nevada batholith (e.g., Barth et al., 2013; Paterson and Ducea, 2015), with peaks in the Triassic, Jurassic, and Cretaceous (Fig. 9). From these data, it appears likely that local sources along the eastern side of the batholith, to the west and north of Death Valley, where Triassic batholithic rocks are present, contributed sediment to the region. Prior to 36 Ma, the arrival of different detritus within the section is consistent with derivation from an
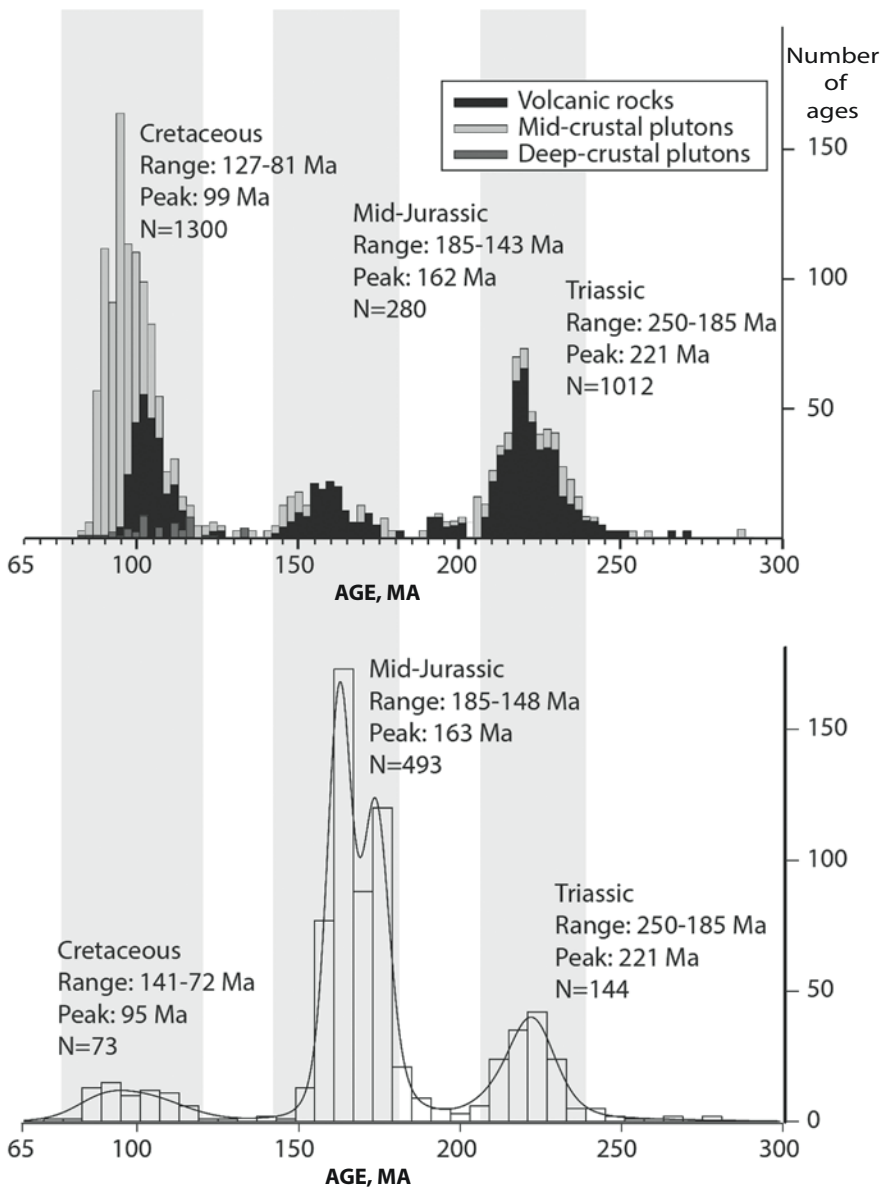

Figure 9. Comparison of Mesozoic detrital zircon ages compiled from selected samples of the Titus Canyon Formation, Death Valley (lower panel; data from this study), against the compiled bedrock ages of Sierra Nevada magmatic rocks (upper panel) from Paterson and Ducea (2015).

extraregional source, as first proposed by Fridrich and Thompson (2011). Our identification of clast types derived from the Roberts Mountains and Golconda allochthons in central and northern Nevada, together with Eocene–Oligocene–age zircons in these strata, implies a northern source region at the latitude of Austin and Ely in northern Nevada. There, caldera complexes developed during the late Eocene and Oligocene across an erosional surface above the Roberts Mountains and Golconda allochthons (Fig. 2).

Consistent with findings by Lund Snee and Miller (this volume), the new data discussed here support the interpretation that voluminous Cenozoic volcanism and plutonism associated with the ignimbrite flareup caused contemporaneous thermal uplift and the formation of topographic relief in the northern Great Basin, providing new sediment source areas for the detritus present in the early Titus Canyon Formation (Fig. 4). In general, the Titus Canyon Formation, its overlying units, and correlative strata contain increasing proportions of volcanic material with ages decreasing upward to 13–12 Ma. As suggested by Fridrich and Thompson (2011), this likely reflects the southward migration of volcanism through time toward the Death Valley–Las Vegas area (Fig. 2).

Although rapid extension related to Basin and Range faulting is reported to have initiated ca. 16 Ma to the east and migrated to Death Valley by 12 Ma (Fridrich and Thompson, 2011), previous workers have suggested that deposition of the Eocene–Oligocene Titus Canyon Formation occurred in a normal fault–bounded basin, thus documenting an episode of much earlier extension in the Death Valley region (e.g., Reynolds, 1969; Saylor, 1991; Niemi, 2002; Snow and Lux, 1999). The evidence that sediment deposited within the Titus Canyon Formation was derived from extraregional sources from the north and the fairly broad distribution of deposits of this age in the Death Valley area (Fridrich and Thompson, 2011) are inconsistent with deposition within a hanging-wall basin of an Eocene–Oligocene normal fault system. In addition, geologic relations in the klippe of the Boundary Canyon fault in the central Funeral Mountains (Figs. 3 and 7) indicate that strata as young as 13–12 Ma were involved in faulting and tilting, with consistent dips throughout the sections (Fig. 7), contrary to what would be expected if these Cenozoic sediments had been deposited during active normal faulting (Raftrey, 2020). These relations provide an additional line of reasoning to support deposition of the Titus Canyon Formation, its overlying units, and their correlatives entirely prior to the onset of faulting in the Death Valley region, as suggested by Fridrich and Thompson (2011). Although additional work is necessary to further characterize the sedimentology and depositional environments of the Titus Canyon Formation and its overlying units and their correlatives, our studies show that their sedimentary packages, at multiple scales, are often lenticular, exhibit significant lateral variability, and contain internal erosional surfaces involving truncation of stratigraphic boundaries and incision of older units by younger units, observations that are consistent with the interpretation of Fridrich and Thompson (2011), i.e., that these represent fluvial sequences deposited in a series of channels that deliv-ered sediments carried by high-energy rivers and streams onto a broad, low-relief alluvial floodplain characterized by intermittent lacustrine environments. As such, the Titus Canyon Formation, its overlying units, and their correlatives represent mostly sediment bypass of Death Valley, with transport toward the Mojave region, which lay near sea level at that time (Cox, 1982; Cox and Diggles, 1986; Lechler and Niemi, 2011).

The provenance of the sandstones and conglomerates that compose the Titus Canyon Formation, overlying units, and their correlatives was from the north, a region commonly believed to have been part of the Nevadaplano (Figs. 1 and 2). The specific timing of the onset of sediment delivery southward to and across the Death Valley region is now constrained to no earlier than late middle Eocene time (38–37 Ma based on fossils dated by Lander, 2019) and not much later than ca. 36 Ma based on the MDAs of sediment shed from the north as determined by the detrital zircon data presented here. This suggests that the documented change in topographic gradient and source regions was not linked to the history of earlier Cretaceous crustal thickening and the contemporaneous formation of the hypothetical Nevadaplano, but it was instead related to the Eocene onset of ignimbrite flareup volcanism across north-central Nevada (Fig. 2). Our data thus support a change in paleogeography of the arc and retro-arc region from one where the continental divide lay along the axis of the Cretaceous magmatic arc throughout Late Cretaceous and Paleocene time (e.g., Van Buer et al., 2009) to one where the continental divide moved eastward toward central Nevada in the Eocene (e.g., Henry and John, 2013; Lund Snee and Miller, this volume; Fig. 2 herein). Magmatism, which began in northern Nevada in Eocene time, contributed to thermally driven uplift and added material to the crustal column mostly before significant extension occurred across the retro-arc region and hypothetical Nevadaplano during Neogene Basin and Range faulting (e.g., summary by Konstantinou and Miller, 2015). The front of this magmatically induced topography migrated southward with time to Las Vegas, fundamentally changing the paleogeography of the west prior to the onset of Basin and Range faulting.

ACKNOWLEDGMENTS

of the manuscript. Any use of trade, firm, or product names is for descriptive purposes only and does not imply endorsement by the U.S. government.

REFERENCES CITED

Barth, A.P., Wooden, J.L., Jacobsen, C.E., and Economos, R.C., 2013, Detrital zircon as a proxy for tracking the magmatic arc system: The California arc example: Geology, v. 41, p. 223–226, https://doi.org/10.1130/G33619.1.

Best, M.G., Barr, D.L., Christiansen, E.H., Gromme, S., Deino, A.L., and Tingey, D.G., 2009, The Great Basin Altiplano during the middle Cenozoic ignimbrite flareup: Insights from volcanic rocks: International Geology Review, v. 51, p. 589–633, https://doi.org/10.1080/00206810902867690.

Best, M.G., Christiansen, E.H., and Gromme, S., 2013, Introduction: The 36–18 Ma southern Great Basin, USA, ignimbrite province and flareup: Swarms of subduction-related supervolcanoes: Geosphere, v. 9, p. 260–274, https://doi.org/10.1130/GES00870.1.

Cassel, E.J., Graham, S.A., and Chamberlain, C.P., 2009, Cenozoic tectonic and topographic evolution of the northern Sierra Nevada, California, through stable isotope paleoaltimetry in volcanic glass: Geology, v. 37, p. 547–550, https://doi.org/10.1130/G25572A.1.

Cassel, E.J., Smith, M.E., and Jicha, B.R., 2018, The impact of slab rollback on Earth's surface: Uplift and extension in the hinterland of the North American Cordillera: Geophysical Research Letters, v. 45, p. 10,996–11,004, https://doi.org/10.1029/2018GL079887.

Chase, C.G., Gregory-Wodzicki, K., Parrish, J.T., and DeCelles, P.G., 1998, Topographic history of the western Cordillera of North America and controls on climate, *in* Crowley, T.J., and Burke, K., eds., Tectonic Boundary Conditions for Climate Reconstructions: Oxford Monographs on Geology and Geophysics 39, p. 73–99.

Colgan, J.P., and Henry, C.D., 2009, Rapid middle Miocene collapse of the Mesozoic orogenic plateau in north-central Nevada: International Geology Review, v. 51, p. 920–961, https://doi.org/10.1080/00206810903056731.

Colgan, J.P., Howard, K.A., Fleck, R.J., and Wooden, J.L., 2010, Rapid middle Miocene extension and unroofing of the southern Ruby Mountains, Nevada: Tectonics, v. 29, no. 6, TC6022, https://doi.org/10.1029/2009TC002655.

Cornwall, H.R., and Kleinhampl, F.J., 1964, Geology of Bullfrog Quadrangle and Ore Deposits Related to Bullfrog Hills Caldera, Nye County, Nevada, and Inyo County, California: U.S. Geological Survey Professional Paper 454-J, 25 p., https://doi.org/10.3133/pp454J.

Coutts, D.S., Matthews, W.A., and Hubbard, S.M., 2019, Assessment of widely used methods to derive depositional ages from detrital zircon populations: Geoscience Frontiers, v. 10, p. 1421–1435, https://doi.org/10.1016/j.gsf.2018.11.002.

Cox, B.F., 1982, Stratigraphy, Sedimentology, and Structure of the Goler Formation (Paleocene), El Paso Mountains, California: Implications for Paleogene Tectonism on the Garlock Fault Zone [Ph.D. dissertation]: Riverside, California, University of California–Riverside, 248 p.

Cox, B.F., and Diggles, M.F., 1986, Geologic Map of the El Paso Mountains Wilderness Study Area, Kern County, CA: U.S. Geological Survey Map MF-1827, 13 p. pamphlet, 1 sheet, scale 1:24,000, https://doi.org/10.3133/mf1827.

DeCelles, P.G., 2004, Late Jurassic to Eocene evolution of the Cordilleran thrust belt and foreland basin system, western U.S.A.: American Journal of Science, v. 304, p. 105–168, https://doi.org/10.2475/ajs.304.2.105.

Dickinson, W.R., and Gehrels, G.E., 2009, Use of U-Pb ages of detrital zircons to infer maximum depositional ages of strata: A test against a Colorado Plateau Mesozoic database: Earth and Planetary Science Letters, v. 288, p. 115–125, https://doi.org/10.1016/j.epsl.2009.09.013.

Dickinson, W.R., Harbaugh, D.W., Saller, A.H., Heller, P.L., and Snyder, W.S., 1983, Detrital modes of Upper Paleozoic sandstones derived from the Antler orogen in Nevada: Implications for the nature of the Antler orogeny: American Journal of Science, v. 283, p. 481–509, https://doi.org/10.2475/ajs.283.6.481.

Farmer, G.L., and DePaolo, D.J., 1983, Origin of Mesozoic and Tertiary granite in the western United States and implications for pre-Mesozoic crustal structure: 1. Nd and Sr isotopic studies in the geocline of the northern Great Basin: Journal of Geophysical Research, v. 88, p. 3379–3401, https://doi.org/10.1029/JB088iB04p03379.

Fridrich, C.J., and Thompson, R.A., 2011, Cenozoic Tectonic Reorganizations of the Death Valley Region, Southeast California and Southwest Nevada: U.S. Geological Survey Professional Paper 1783, 36 p., https://doi.org/10.3133/pp1783.

Fridrich, C.J., Thompson, R.A., Slate, J.L., Berry, M.E., and Machette, M.N., 2012, Geologic Map of the Southern Funeral Mountains Including Nearby Groundwater Discharge Sites in Death Valley National Park, California and Nevada: U.S. Geological Survey Scientific Investigations Map 3151, 20 p. pamphlet, 1 sheet, scale 1:50,000, https://doi.org/10.3133/sim3151.

Gehrels, G.E., 2013, Calculating Maximum Depositional Ages: https://sites.google.com/a/laserchron.org/laserchron/ (accessed 1 December 2019).

Gehrels, G., and Pecha, M., 2014, Detrital zircon U-Pb geochronology and Hf isotope geochemistry of Paleozoic and Triassic passive margin strata of western North America, Geosphere, v. 10, p. 49–65, https://doi.org/10.1130/GES00889.1.

Gehrels, G.E., Valencia, V.A., and Ruiz, J., 2008, Enhanced precision, accuracy, efficiency, and spatial resolution of U-Pb ages by laser ablation–multicollector–inductively coupled plasma–mass spectrometry: Geochemistry Geophysics Geosystems, v. 9, Q03017, https://doi.org/10.1029/2007GC001805.

Graber, K.K., and Chafetz, H.S., 1990, Petrography and origin of bedded barite and phosphate in the Devonian Slaven Chert of central Nevada: Journal of Sedimentary Research, v. 60, p. 897–911, https://doi.org/10.1306/D4267640-2B26-11D7-8648000102C1865D.

Harbaugh, D.W., and Dickinson, W.R., 1981, Depositional facies of Mississippian clastics, Antler foreland basin, central Diamond Mountains, Nevada: Journal of Sedimentary Research, v. 51, p. 1223–1234, https://doi.org/10.1306/212F7E6E-2B24-11D7-8648000102C1865D.

Henry, C.D., 2008, Ash-flow tuffs and paleovalleys in northeastern Nevada: Implications for Eocene paleogeography and extension in the Sevier hinterland, northern Great Basin: Geosphere, v. 4, p. 1–35, https://doi.org/10.1130/GES00122.1.

Henry, C.D., and John, D.A., 2013, Magmatism, ash-flow tuffs, and calderas of the ignimbrite flareup in the western Nevada volcanic field, Great Basin, USA: Geosphere, v. 9, no. 4, p. 951–1008, https://doi.org/10.1130/GES00867.1.

Henry, C.D., Hinz, N.H., Faulds, J.E., Colgan, J.P., John, D.A., Brooks, E.R., Cassel, E.J., Garside, L.J., Davis, D.A., and Castor, S.B., 2012, Eocene–early Miocene paleotopography of the Sierra Nevada–Great Basin–Nevadaplano based on widespread ash-flow tuffs and paleovalleys: Geosphere, v. 8, p. 1–27, https://doi.org/10.1130/GES00727.1.

Hunt, C.B., and Mabey, D.R., 1966, Stratigraphy and Structure, Death Valley, California: U.S. Geological Survey Professional Paper 494-A, 162 p., https://doi.org/10.3133/pp494A.

Konstantinou, A., and Miller, E.L., 2015, Evidence for a long-lived accommodation/transfer zone beneath the Snake River Plain: A possible influence on Neogene magmatism?: Tectonics, v. 34, p. 2387–2398, https://doi.org/10.1002/2015TC003863.

Lander, E.B., 2019, Early late Duchesnean (late middle Eocene) Titus Canyon fauna, Titus Canyon Formation, Death Valley National Park, Inyo County, southeastern California, *in* Miller, D.M., ed., Exploring Ends of Eras in the Eastern Mojave Desert, Desert Symposium Field Guide and Proceedings: Desert Hot Springs, California, Desert Symposium Inc., p. 141–153, http://www.desertsymposium.org/DS%202019%20Ends%20of%20Eras%20small.pdf.

Lechler, A.R., and Niemi, N.A., 2011, Sedimentologic and isotopic constraints on the Paleogene paleogeography and paleotopography of the southern Sierra Nevada, California: Geology, v. 39, p. 379–382, https://doi.org/10.1130/G31535.1.

Lechler, A.R., Niemi, N.A., Hren, M.T., and Lohmann, K.C., 2013, Paleoelevation estimates for the northern and central proto–Basin and Range from carbonate clumped isotope thermometry: Tectonics, v. 32, p. 295–316, https://doi.org/10.1002/tect.20016.

Lee, J., Blackburn, T., and Johnston, S., 2017, Timing of mid-crustal ductile extension in the northern Snake Range metamorphic core complex, Nevada: Evidence from U/Pb zircon ages: Geosphere, v. 13, p. 439–459, https://doi.org/10.1130/GES01429.1.

Lofgren, D.L., Honey, J.G., McKenna, M.C., Zondervan, R.L., and Smith, E.E., 2008, Paleocene primates from the Goler Formation of the Mojave Desert in California, *in* Wang, X., and Barnes, L.G., eds., Geology and Vertebrate Paleontology of Western and Southern North America: Contributions in Honor of David P. Whistler: Los Angeles, California, Natural History Museum of Los Angeles County, p. 11–28.

Long, S.P., 2012, Magnitudes and spatial patterns of erosional exhumation in the Sevier hinterland, eastern Nevada and western Utah, USA: Insights

from a Paleogene paleogeologic map: Geosphere, v. 8, p. 881–901, https://doi.org/10.1130/GES00783.1.

Lund Snee, J.E., and Miller, E.L., 2022, this volume, Magmatism, migrating topography, and the transition from Sevier shortening to Basin and Range extension, western United States, *in* Craddock, J.P., Malone, D.H., Foreman, B.Z., and Konstantinou, A., eds., Tectonic Evolution of the Sevier-Laramide Hinterland, Thrust Belt, and Foreland, and Postorogenic Slab Rollback (180–20 Ma): Geological Society of America Special Paper 555, https://doi.org/10.1130/2021.2555(13).

Mattinson, C.G., Colgan, J.P., Metcalf, J.R., Miller, E.L., and Wooden, J.L., 2007, Late Cretaceous to Paleocene metamorphism and magmatism in the Funeral Mountains metamorphic core complex, Death Valley, California, *in* Cloos, M., Carlson, W.D., Gilbert, M.C., Liou, J.G., and Sorensen, S.S., eds., Convergent Margin Terranes and Associated Regions: A Tribute to W.G. Ernst: Geological Society of America Special Paper 419, p. 205–223, https://doi.org/10.1130/2006.2419(11).

McQuarrie, N., and Chase, C.G., 2000, Raising the Colorado Plateau: Geology, v. 28, p. 91–94, https://doi.org/10.1130/0091-7613(2000)028<0091:RTCP>2.0.CO;2.

Miller, E.L., and Larue, D.K., 1983, Ordovician quartzite in the Roberts Mountains allochthon, Nevada: Deep sea fan deposits derived from cratonal North America, *in* Stevens, C.H., ed., Pre-Jurassic Rocks in Western North American Suspect Terranes: Los Angeles, California, Pacific Section, Society of Economic Paleontologists and Mineralogists, p. 91–102.

Miller, E.L., Holdsworth, B.K., Whiteford, W.B., and Rodgers, D., 1984, Stratigraphy and structure of the Schoonover sequence, northeastern Nevada: Implications for Paleozoic plate-margin tectonics: Geological Society of America Bulletin, v. 95, no. 9, p. 1063–1076, https://doi.org/10.1130/0016-7606(1984)95<1063:SASOTS>2.0.CO;2.

Mix, H.T., Mulch, A., Kent-Corson, M.L., and Chamberlain, C.P., 2011, Cenozoic migration of topography in the North American Cordillera: Geology, v. 39, p. 87–90, https://doi.org/10.1130/G31450.1.

Niemi, N.A., 2002, Extensional Tectonics in the Basin and Range Province and the Geology of the Grapevine Mountains, Death Valley Region, California and Nevada [Ph.D. thesis]: Pasadena, California, California Institute of Technology, 344 p.

Niemi, N.A., 2012, Geologic Map of the Central Grapevine Mountains, Inyo County, California, and Esmeralda and Nye Counties, Nevada: Geological Society of America Digital Map and Chart Series 12, scale 1:48,000, https://doi.org/10.1130/2012.DMCH012.

Oldow, J.S., 1984, Spatial variability in the structure of the Roberts Mountains allochthon, western Nevada: Geological Society of America Bulletin, v. 95, p. 174–185, https://doi.org/10.1130/0016-7606(1984)95<174:SVITSO>2.0.CO;2.

Parsons, T., Thompson, G.A., and Sleep, N.H., 1994, Mantle plume influence on the Neogene uplift and extension of the U.S. western Cordillera?: Geology, v. 22, p. 83–86, https://doi.org/10.1130/0091-7613(1994)022<0083:MPIOTN>2.3.CO;2.

Paterson, S.R., and Ducea, M.N., 2015, Arc magmatic tempos: Gathering the evidence: Elements, v. 11, no. 2, p. 91–98, https://doi.org/10.2113/gselements.11.2.91.

Raftrey, M.E., 2020, Character and Timing of Deformation in the Funeral Mountains Metamorphic Core Complex, Death Valley, California and Nevada [M.S. thesis]: Stanford, California, Stanford University, https://purl.stanford.edu/nt476zw6922.

Reid, S.A., 1988, Late Cretaceous and Paleocene sedimentation along the east side of the San Joaquin basin, *in* Graham, S.A., ed., Studies of the Geology of the San Joaquin Basin: Late Cretaceous and Paleocene Sedimentation along the East Side of the San Joaquim Basin: Bakersfield, California, Pacific Section, American Association of Petroleum Geologists Bulletin, v. 70, p. 157–171.

Reynolds, M.W., 1969, Stratigraphy and Structural Geology of the Titus and Titanothere Canyons Area, Death Valley, California [Ph.D. thesis]: Berkeley, California, University of California–Berkeley, 310 p.

Saleeby, J., Farley, K.A., Kistler, R.W., and Fleck, R., 2007, Thermal evolution and exhumation of deep level batholithic exposures, southernmost Sierra Nevada, California, *in* Cloos, M., Carlson, W.D., Gilbert, M.C., Liou, J.G., and Sorensen, S.S., eds., Convergent Margin Terranes and Associated Regions: A Tribute to W.G. Ernst: Geological Society of America Special Paper 419, p. 39–66, https://doi.org/10.1130/2007.2419(02).

Saylor, B.Z., 1991, The Titus Canyon Formation: Evidence for Early Oligocene Extension in the Death Valley Area, California [M.S. thesis]: Cambridge, Massachusetts, Massachusetts Institute of Technology, 65 p., http://hdl.handle.net/1721.1/31027.

Sharman, G.R., Graham, S.A., Grove, M., Kimbrough, D.L., and Wright, J.E., 2015, Detrital zircon provenance of the Late Cretaceous–Eocene California forearc: Influence of Laramide low-angle subduction on sediment dispersal and paleogeography: Geological Society of America Bulletin, v. 127, p. 38–60, https://doi.org/10.1130/B31065.1.

Snow, J.K., and Lux, D.R., 1999, Tectono-sequence stratigraphy of Tertiary rocks in the Cottonwood Mountains and northern Death Valley area, California and Nevada, *in* Wright, L.A., and Troxel, B.W., eds., Cenozoic Basins of the Death Valley Region: Geological Society of America Special Paper 333, p. 17–64, https://doi.org/10.1130/0-8137-2333-7.17.

Sonder, L.J., England, P.C., Wernicke, B.P., and Christiansen, R.L., 1987, A physical model for Cenozoic extension of western North America, *in* Coward, M.P., Dewey, J.F., and Hancock, P.L., eds., Continental Extensional Tectonics: Geological Society, London, Special Publication 28, p. 187–201, https://doi.org/10.1144/GSL.SP.1987.028.01.14.

Stewart, J.H., 1980, Geology of Nevada: Geological Society of Nevada Special Publication 4, 136 p.

Stock, C., and Bode, F.D., 1935, Occurrence of Lower Oligocene mammal bearing beds near Death Valley, California: Proceedings of the National Academy of Sciences of the United States of America, v. 21, p. 571–579, https://doi.org/10.1073/pnas.21.10.571.

Sundell, K., 2019, Laser Ablation ICP-MS Data Reduction Software from the Arizona LaserChron Center: https://www.kurtsundell.com/agecalcml-updates (accessed 20 August 2021).

Tomlinson, A.J., 1991, Biostratigraphy, Stratigraphy, Sedimentary Petrology, and Structural Geology of the Upper Paleozoic Golconda Allochthon, North-Central Nevada [Ph.D. thesis]: Stanford, California, Stanford University, 482 p., scale 1:10,000.

U.S. Geological Survey, 1988a, Chloride City Quadrangle California–Inyo Co. Topographic Quadrangle Map: U.S. Geological Survey 7.5 Minute Series, scale 1:24,000.

U.S. Geological Survey, 1988b, Daylight Oass, CA-NV 7.5′ Topographic Quadrangle Map: U.S. Geological Survey 7.5 Minute Series, scale 1:24,000.

U.S. Geological Survey, 1988c, Thimble Peak, Calif.–Nev. 7.5′ Topographic Quadrangle Map: U.S. Geological Survey 7.5 Minute Series, scale 1:24,000.

Van Buer, N.J., and Miller, E.L., 2010, Sahwave batholith, NW Nevada: Cretaceous arc flare-up in a basinal terrane: Lithosphere, v. 2, p. 423–446, https://doi.org/10.1130/L105.1.

Van Buer, N.J., Miller, E.L., and Dumitru, T.A., 2009, Early Tertiary paleogeologic map of the northern Sierra Nevada batholith and the northwestern Basin and Range: Geology, v. 37, no. 4, p. 371–374, https://doi.org/10.1130/G25448A.1.

Vermeesch, P., 2018, IsoplotR: A free and open toolbox for geochronology: Geoscience Frontiers, v. 9, p. 1479–1493, https://doi.org/10.1016/j.gsf.2018.04.001.

Wells, M.L., Hoisch, T.D., Cruz-Uribe, A.M., and Vervoort, J.D., 2012, Geodynamics of synconvergent extension and tectonic mode switching: Constraints from the Sevier-Laramide orogen: Tectonics, v. 31, TC1002, https://doi.org/10.1029/2011TC002913.

Wolfe, J.A., Forest, C.E., and Molnar, P., 1998, Paleobotanical evidence of Eocene and Oligocene paleoaltitudes in midlatitude western North America: Geological Society of America Bulletin, v. 110, p. 664–678, https://doi.org/10.1130/0016-7606(1998)110<0664:PEOEAO>2.3.CO;2.

Workman, J.B., Menges, C.M., Page, W.R., Taylor, E.M., Ekren, E.B., Rowley, P.D., and Wright, L.A., 2002, Geologic Map of the Death Valley Ground-Water Model Area, Nevada and California: U.S. Geological Survey Miscellaneous Field Studies Map MF-2381-A, scale 1:250,000, https://doi.org/10.3133/mf2381A.

Wright, L.A., and Troxel, B.W., 1993, Geologic Map of the Central and Northern Funeral Mountains and Adjacent Areas, Death Valley Region, Southern California: U.S. Geological Survey Miscellaneous Investigations Map I-2305, scale 1:48,000, https://doi.org/10.3133/i2305.

Printed in the USA